Silurian to Devonian magmatism, molybdenite mineralization, regional exhumation and brittle strike-slip deformation along the Loch Shin Line, NW Scotland.

Holdsworth, R.E.[1], Dempsey, E.[1], Selby, D.[1], Darling, J.R.[2], Feely, M.[3], Costanzo, A.[3], Strachan, R.A.[2], Waters, P.[4], Finlay, A.J.[5]

1=Department of Earth Sciences, Durham University, Durham, UK, DH1 3LE.
2= School of Earth and Environmental Sciences, University of Portsmouth, Portsmouth, PO1 3QL.
3= Earth and Ocean Sciences, School of Natural Sciences, Quadrangle Building, National University of Ireland, Galway, Ireland.
4=Eurasian Consolidated Minerals Pty Ltd, Level 1, 415 Riverside Road, Hawthorn East, Victoria 3123, Australia.
5=Chemostat, 1 Ravenscroft Court, Buttington Enterprise Park, Welshpool, SY21 8SL, UK.

ABSTRACT

The Loch Shin Line (LSL) is a geological-geophysical lineament associated with an anomalous zone of mantle-derived appinites, granites and strike-slip faulting that runs NW-SE across the Moine Nappe from the Moine Thrust to the Moray Firth. U-Pb zircon and Re-Os molybdenite dating of the Loch Shin and Grudie plutons that lie to immediately south of the NW-SE Loch Shin-Strath Fleet fault system yields ca 427-430Ma ages that overlap within error. They also coincide with previously obtained U-Pb zircon ages for the Rogart pluton which lies along strike to the southeast. Field and microstructural observations confirm the similarity and contemporaneous nature of the plutons and associated sulphide mineralisation. Fluid inclusion analyses place further constraints on the P-T-X conditions during regional late Caledonian exhumation of the Moine Nappe in this part of NW Scotland. Synchronous to slightly younger (ca 410Ma?) brittle dextral strike slip faulting along the WNW-ESE Loch Shin-Strath Fleet Fault System was likely antithetic to regional sinistral strike-slip movements along the NE-SW trending Great Glen Fault. Our findings lend support to the hypothesis that the LSL acted as a deep crustal

channelway controlling the ascent and emplacement of Silurian granitic and appinitic magmas into the overlying Moine Nappe. We propose that this deep structure corresponds to the southeastern continuation of the Precambrian-age Laxford Front shear zone in the buried Lewisian autochthon.

INTRODUCTION

It is well established that orogenic belts worldwide are characterized by interlinked systems of thrust, strike slip and extensional faults and, at deeper crustal levels, by shear zones that collectively accommodate crustal deformation during plate collision (e.g. Dewey *et al.* 1986). In general, this leads to the development of broad, diffuse regions of 'block and flake tectonics' where plate motions are partitioned into complex displacements, internal strains and rotations. The location, geometry and persistence of faults and shear zones in such regions are known to be influenced directly by the presence and reactivation of crustal-scale pre-existing structures (Sutton & Watson 1986; Holdsworth *et al.* 1997, 2001). These same structures are also known to act as channelways that control the upward migration and emplacement of hydrous mineralizing fluids and magmas (e.g. O'Driscoll 1986; Hutton 1988a; Jacques & Reavy 1994; Richards 2013). This coincidence of geological processes has greatly assisted in the analysis of orogenic deformation histories worldwide since dating of igneous intrusions and/or mineralization events using geochronology can also be used to constrain the absolute ages of associated deformation events in the adjacent wall rocks (e.g. Paterson & Tobisch 1988; Schofield & D'Lemos 1998; Rosenberg 2004).

Integrated structural and geochronological studies of deformed igneous intrusions have played a key role in constraining the timing of events within the Early Palaeozoic Caledonian orogeny in Scotland (Fig. 1a). Following Ordovician arc continent collision (the Grampian event), the final closure of Iapetus involved the oblique collisions of three palaeo-continents: Laurentia, Baltic and Avalonia during the mid- to late Silurian (e.g. Soper *et al.* 1992; Torsvik *et al.* 1996). In NW Scotland, regional deformation occurred due to the sinistral oblique Scandian collision of Baltica with Laurentia. Crustal thickening here was overlapped and followed by major sinistral displacements along orogen-parallel strike-slip faults such as the Great Glen Fault (GGF; Fig 1a) heralding a transition from a regime of sinistral transpression to transtension (Dewey & Strachan 2003 and references therein). Igneous activity and associated mineralization related to slab breakoff was associated with every stage of this transition, with earlier granites syn-tectonically emplaced along Scandian thrusts (e.g. Naver Thrust, see Holdsworth & Strachan 1988; Kinny et al 2003; Goodenough *et al.* 2011; Kocks *et al.* 2013), whilst later, volumetrically larger volumes of melt were emplaced along steeply-dipping strike-slip or normal faults (e.g. Great Glen Fault; Hutton 1988b; Hutton & McErlean 1991; Jacques & Reavy, 1994; Stewart *et al.* 2001). In many cases the controlling faults or shear zones are exposed at the present-day surface, but others are more enigmatic features. As illustrated by Jacques & Reavy (1994) they are commonly inferred 'buried' structures based on geological, geophysical or geochemical alignments that define regional scale transverse lineaments that run generally at high angles to the orogenic strike. One of these NW-SE features, the Loch Shin Line (LSL) – first defined by Watson (1984) – is associated with an anomalous zone of mantle-derived appinites, granites and brittle faulting in the Moine Nappe SE of the Moine Thrust on the N side of the Assynt culmination (Fig. 1a, b). The LSL follows a strong NW-SE gravity gradient that defines the NE margin of a strong negative anomaly centred on the Grudie Granite (Figs 1b, see Leslie *et al.* 2010 and references therein). Watson (1984) suggested that the LSL corresponds to the presence of a Precambrian shear zone in the Lewisian autochthon underlying the Moine Nappe and that this shear zone has controlled the siting and ascent of magmas and associated mineralization during the Silurian. The dextral faulting that follows the trend of the LSL defines the Loch Shin, Strath Fleet and Dornoch Firth fault systems (Fig. 2a; Strachan & Holdsworth 1988) which are thought to be part of a regional fault set antithetic to the regional sinistral movements along faults such as the GGFZ (see Johnson & Frost 1977; Watson 1984). The Rogart igneous complex (Fig. 1a; Soper 1963), a large composite igneous intrusion of mantle derivation that lies on the NE margin of the LSL, is bounded to the SW by the Strath Fleet Fault. Kocks *et al.* (2013) have shown that emplacement of the central pluton – dated at 425±1.5 Ma using U-Pb (TIMS) zircon - was likely controlled by dextral motions along the LSL. These authors used this evidence to date the switch from sinistral transpression with thrusting to transtension with regional strike slip faulting at ca. 425 Ma.

The present paper re-examines this hypothesis in the region of Loch Shin where two plutons notably associated with a zone of molybdenite mineralization hosted in Moine and Lewisian country rocks (Gallagher & Smith 1976) are poorly exposed: the Loch Shin and Grudie granites (Figs 1 & 2). Field observations and microstructural studies are used to constrain the geometry, kinematics and relative ages of deformation in the plutons and country rocks, whilst U-Pb zircon and Re-Os molybdenite geochrology are used to date both pluton emplacement and the spatially associated mineralization. Finally, fluid inclusion studies are used to further constrain the P-T-X conditions during deformation and igneous emplacement and assess the relationships between regional structures such as the LSL and fluid flow.

GEOLOGICAL SETTING

The Loch Shin area is mostly underlain by variably deformed metsedimentary rocks of the Morar Group, part of the Neoproterozoic Moine Supergroup in NW Scotland (Figs 1, 2; Holdsworth *et al.* 1994; Strachan *et al.* 2010). To the northwest, the Moine Nappe is bounded by the underlying Moine Thrust and Moine Thrust Zone, whilst to the north and east it is overlain by the Naver Thrust which carries the Loch Coire Migmatite Complex (Fig. 1a; Kocks *et al.* 2013). Zircon U-Pb geochronology shows that the migmatite complex formed during the Ordovician Grampian event ca 470-460Ma (Kinny *et al.* 1999). This was then followed by generally top-to-the-NW Scandian ductile thrusting with early displacement along the Naver Thrust, followed by later thrusts propagating progressively towards the Caledonian foreland ending with the development of the Moine Thrust Zone (Barr *et al.* 1986; Johnson & Strachan 2006; Alsop *et al.* 2010; Leslie *et al.* 2010). Zircon U-Pb dating of various syn-kinematic igneous intrusions constrains thrust movements to have occurred ca. 435-425Ma (Kinny et al .2003; Kocks *et al.* 2006; Goodenough *et al.* 2011). The broad regional arcuate swing of the regional foliation and ductile thrusts within the Moine and Naver nappes (Fig. 1a, 2a) is attributed to the development of the Cassley structural culmination and regional-scale flexuring in the rocks overlying the Assynt thrust culmination (Elliott & Johnson 1980; Butler & Coward 1984; Leslie *et al.* 2010).

The Loch Shin and Grudie granites are hosted in Moine Supergroup rocks belonging to the Morar Group which are locally interleaved with antiformal isoclinal infolds of their underlying Lewisianoid basement (Read *et al.* 1926; Gallagher & Smith 1976; Strachan & Holdsworth 1988; Leslie *et al.* 2010). The Moine rocks are mostly unmignmatized psammites interlayered with subordinate semipelitic and pelitic horizons preserving rare sedimentary structures such as cross-lamination and grading in areas of low tectonic strain. The Lewisianoid rocks are typically lithologically diverse and include hornblendic and quartzofeldspathic gneisses, amphibolites and subordinate units of ultramafic hornblendite, together with thin strips of metasedimentary schist and marble (e.g. as seen on the Airde of Shin, Fig. 2a; Strachan & Holdsworth 1988 and references therein). Individual Moine-Lewisianoid boundaries – where exposed - are marked either by the development of local basement conglomerates or by the development of mica-rich 'tectonic schists' (e.g. Airde of Shin; Fig 2a) (Peacock 1975; Strachan & Holdsworth 1988).

The dominant structures in the Moine and Lewisianoid rocks are tight to isoclinal D2 folds that carry an axial planar S2 crenulation fabric of an earlier bedding parallel schistosity (S1). The main foliation is therefore in general a composite S0/S1/S2 fabric which carries an ESE- to SE-plunging mineral extension lineation L2 (Strachan & Holdsworth 1988). This lineation is interpreted to lie parallel to the regional direction of top-to-the-NW tectonic transport during Scandian thrusting (e.g. Barr *et al.* 1986; Strachan *et al.* 2010). Associated regional metamorphism during D2 in the Loch Shin area was within the low to mid-amphibolite facies (Soper & Brown 1971; Strachan & Holdsworth 1988).

The Moine and Lewisianoid rocks around Lairg and Loch Shin are cut by a number of granitic bodies, which include (from largest to smallest): the Grudie, Claonel and Loch Shin intrusions (Fig. 2; Gallagher & Smith 1976), together with numerous small associated sheets and plugs of similar composition. These fall into two distinct groups: early foliated granodiorites (Claonel), thought to be directly equivalent to parts of the Rogart igneous complex, and supposedly later, generally unfoliated intrusions of pink adamellite including the Grudie and Loch Shin bodies. The trace of the LSL is also marked by a concentration of small plugs and pipe-like bodies of intermediate to ultramafic appinites known locally as the Ach'uaine hybrids (Fig. 1b; Read *et al.* 1925; Watson 1984). These also occur as comagmatic enclaves within the ca. 425Ma central granodiorite of the Rogart igneous complex (Fowler *et al.* 2001; Kocks *et al.* 2013). Appinitic intrusions are widely associated with late Caledonian plutons throughout the Scottish Highlands and point to a significant mantle contribution to this magmatism (e.g. see Fowler & Henney 1996; Fowler *et al.* 2008).

Regional mapping, stream sediment sampling and analysis of shallow borehole cores in the Loch Shin-Grudie area has shown that low grade molybdenite mineralization is associated with pyrite in thin post-foliation quartz veins cutting both country rock and granites; subordinate chalcopyrite, fluorite, galena, barite and sphalerite also occur (Gallagher & Smith 1976). This mineralization is spatially associated with the granites, but Gallagher & Smith (op cit) suggest that it may also have been significantly influenced by regional structures in the surrounding wall rocks.

Between Loch Shin and the Moray Firth to the east, the Moine and Lewisian rocks are cut by at least three major, sub-vertical brittle faults: the Loch Shin, Strath Fleet and Dornoch Firth fault zones (Fig. 1a; Read *et al.* 1925, 1926; Strachan & Holdsworth 1988; Kocks *et al.* 2013). Exposure of the fault zones is generally very poor and only the Strath Fleet fault has been previously studied in any detail (Soper 1963). A series of NW-SE-trending steeply dipping crush zones were recognized that overprint Moine country rocks, the Rogart igneous complex and unconformably overlying Devonian basal conglomerates (middle Old Red Sandstone). There is evidence for multiple fault movements, with cataclastic fault rocks included as clasts within overlying Devonian conglomerates and minor intrusions that cut brittle fault rocks whilst also being overprinted by later faulting (Soper 1963). However, there is little published evidence to support the dextral shear sense inferred by many authors along these NW-SE faults (e.g. Johnson & Frost 1977; Watson 1984), although apparent regional offsets of regional boundaries in the Moine Nappe are consistent with right-lateral movements along the Strath Fleet and Dornoch Firth Faults (Fig 1a; Soper 1963; Strachan & Holdsworth 1988). A presumably late (?Devonian) NE-side-down movement is also inferred for the Strath Fleet Fault based on the preservation of Devonian conglomerates in an elongate NW-SE-trending outlier that follows the Strath Fleet Valley (e.g. see Kocks *et al.* 2013).

There are no published structural studies of any of the igneous bodies that occur close to Loch Shin due to the extremely poor levels of exposure (<1%). The Grudie pluton is inferred to cross-cut all ductile fabrics and geological boundaries in the Moine and Lewisian rocks based on the obviously discordant nature of the mapped boundaries and the absence of an internal foliation (Fig. 2b; Gallagher & Smith 1976). The present study focusses on two key areas of exposure: a ca 1 km long sporadically continuous section through Moine rocks and part of the Loch Shin Granite on the southwest shore of Loch Shin; and isolated exposures of Grudie Granite exposed in road cuts related to the Meall a Gruididh wind farm development (Fig. 2b).

LOCH SHIN GRANITE

Good quality water-washed exposures of Moine country rocks, the Loch Shin Granite and associated mineral veins occur along the SW shore of Loch Shin between NC 5650 0590 and NC 5625 0668 (Fig. 2b). Isolated poor quality exposures also occur in inland areas and stream sections, notably along the Allt a'Chlaonaidh (see Gallagher & Smith 1976, fig. 3).

Moine country rocks are exposed south of the Loch Shin granite between NC 5650 0590 and NC 0623 5638 and, north of the granite, between NC 5625 0668 and NC 5587 0766. They are for the most part fine to medium grained grey mica psammites with a flaggy foliation and mm-scale compositional banding (Fig. 3a).

Isolated layers of grey-brown weathering semipelite-pelite are sparsely developed in layers up to 20cm thick. In thin section, the psammites typically comprise quartz, plagioclase, K feldspar, green biotite and accessory phases (mineralization, garnet, epidote). Quartz and feldspar uniformly display sub-equant polygonal to cuspate-lobate textures typical of amphibolite facies conditions (e.g. see Holdsworth & Grant 1990), with the main banding parallel fabric (S0/S1/S2) being defined primarily by aligned biotite grains (Fig. 3b). The foliation and associated mineral lineations are locally variable in orientation – possibly due to the local effects of late brittle folding and faulting (see below) - but the majority strike NE-SW with moderate SE dips (Figs 2b, 4a). The associated fine mineral lineations, interpreted here as L2, plunge mainly ESE (Fig. 4a) as is typical of this part of the Moine Nappe in Sutherland (e.g. Strachan & Holdsworth 1988).

The ductile foliation in the Moine rocks is cross cut at low angles by a number of generally NE-SW trending, moderately SE dipping pink granite and granite pegmatite sheets up to 1m thick (e.g. Figs 3a, 5b). These are unfoliated and are compositionally very similar to the main Loch Shin granite.

The contacts of the Loch Shin granite are not exposed but are inferred to trend NE-SW and dip to the SE (Figs 2b, 4b). The pink granite is typically fine to medium grained and is unfoliated, lacking both magmatic and solid-state ductile fabrics (Fig. 3c, d). In thin section it typically comprises weakly sericitised plagioclase, perthitic K-feldspar (occasionally as phenocrysts), quartz, biotite (often altered to secondary chlorite) and iron oxide (?magnetite). The granite appears to be fairly homogeneous in terms of both composition and grain size and no internal contacts were seen. No magmatic-state fabric is present, nor is there any evidence of crystal plasticity other than low-temperature features spatially associated with fractures.

The granite is cut by irregular sets of quartz-pyrite-chalcopyrite veins (Fig. 3e) with rare molybdenite. These appear to occur in a variety of orientations and no particular trend seems to dominate. However, at NC 5630 0660, a large subvertical SSE-NNW trending quartz-pyrite-sphalerite-chalcopyrite-galena vein up to 1 m thick is exposed (Fig. 3f) and can be traced for over 10 metres along strike. The veins also lack ductile deformation fabrics, but are cross cut by brittle faults and the effects of low temperature cataclasis (e.g. Fig. 5a). Rice & Cope (1973) and Gallagher & Smith (1976) give further details of veins and mineralization found in the surrounding Moine and Lewisian rocks and report the additional presence of minor amounts of covellite, barytes and fluorspar. Rare, late veins of zeolite <1mm thick were observed cross-cutting fault-related breccias in Moine host rocks (e.g. NC 5625 0668).

Brittle deformation is widely recognized cutting both Moine country rocks, the Loch Shin Granite and associated granite-pegmatite veins (Figs 5a-f). The Loch Shin Granite is cut by a series of steeply-dipping, several metre long, very planar dextral faults trending WNW-ESE with shallowly plunging slickenlines (Figs 4c, 5c). The total offsets are unknown. Dextral faults are everywhere associated with shorter length, steeply-dipping N-S to NE-SW sinistral faults with cm-scale offsets (Figs 4c, 5a) which either abut against or are cross-cut by dextral faults (Fig. 5d) suggesting that they are contemporaneous. A subordinate set of irregularly oriented, mainly shallowly-dipping reverse faults with prominent NNW- to SSE-plunging grooves & slickenlines is locally present in the granite outcrops (e.g. around NC 5635 0630; Figs 4d, 5e). The fault planes are notably curvilplanar & lineated, with a series of ramp-flat configurations. Offsets are mostly small (mm-cm scale). Once again these faults show mutually cross-cutting relationships with the steeply dipping strike slip faults suggesting that they are broadly contemporaneous. A stress inversion analysis of all fault slickenline data suggests a normal faulting to transtensional stress regime with a component of N-S shortening and E-W extension consistent with regional-scale dextral shear along the Loch Shin Fault (Fig 4f).

In addition to brittle faults, both Moine rocks and granite are locally cut by metre-scale zones of brecciation and cataclasis, some of which appear to be associated with specific faults whilst others seem to be diffuse and irregular. The banded Moine rocks locally preserve brittle-ductile box folds with generally moderate to steep easterly plunges (e.g. Figs 4e, 5f). These structures refold the ductile foliation (S2) and lineation (L2). The age of these folds relative to granite emplacement is uncertain, but one example appears to detach along a NE-SW sinistral fault suggesting that the folds are also post-granite features related to the regional brittle deformation. Such folds have not been observed within the granite, but it is suggested that this may be due to a lack of pre-existing mechanical layering in the igneous host rocks.

In thin section, the effects of brittle deformation and cataclasis are widespread in all rocks along the Loch Shin shore section (e.g. Figs 6a-f). Irregular networks of small offset shear and hybrid fractures host variable amounts of mineralization and secondary alteration features including sericite and other clay minerals, quartz, chlorite, hematite, pyrite, chalcopyrite, limonite, fluorite and zeolite (e.g. Figs 6c, e, f). This suggests that the fractures have hosted significant volumes of fluid, an assertion supported by the widespread preservation of multiple sets of healed microfractures (Tuttle lamellae) in quartz in a wide range of orientations (Figs 6d, e). The presence of both pyrite and chalcopyrite in these fracture fills suggest that at least some of the widely observed base metal mineralization was synchronous with brittle deformation. In several cases, sericite-filled fractures cutting feldspars are seen to pass laterally into well-defined Tuttle lamellae in adjacent quartz grains (Fig. 6e). Isolated veins of zeolite <1mm thick cross cut all other brittle structures (Fig. 6f) and appear to represent the final phase of mineralization.

GRUDIE GRANITE

The Grudie Granite is exceptionally poorly exposed and none of its contacts have been observed, although the mapped relationships suggest that it is highly discordant with the foliation in the surrounding Moine and Lewisianoid wall rocks (Fig 2b). In surface exposures, the granite is entirely unfoliated, is medium to fine grained, with sparse large phenocrysts of perthitic K-feldspar up to 1cm across and large rounded xenocrysts of polycrystalline quartz up to 1cm across (Fig. 7a-d). These are set in a matrix of lightly to moderately sericitized plagioclase and quartz, with sparse K-feldspar, biotite and iron oxide. Little internal variation in grain size or mineralogy has been observed and internal contacts were not found.

In the field, well-developed joints carry epidote, chlorite, zeolite, iron and manganese oxides with slickenlines locally developed in a variety of orientations, mainly dip-slip or oblique slip (Fig. 7b). In thin section, the effects of brittle deformation are limited with small fractures filled mainly with epidote, white mica, chlorite and limonite. The overall level of fracturing is much less when compared to the Loch Shin Granite (e.g. Figs 7c, d).

ZIRCON U-Pb ISOTOPE ANALYSIS

Sample, mineral separation and analytical protocols

A representative sample of Loch Shin granite from the SW west shore of Loch Shin (DS1-11; Fig. 2b, NC 5635 0625) was selected for Zircon U-Pb LA-ICP-MS geochronology. Zircons were separated from sample DS1-11 using heavy liquids and an isodynamic magnetic separator. The zircon fraction for analysis was handpicked under a binocular microscope and mounted in epoxy resin along with grains of the zircon reference material Temora 2 (Black *et al.* 2004). After polishing and carbon coating, cathodoluminescence (CL) images of the zircons were taken with a KeDev Centaurus CL detector housed on a JEOL 6060LV SEM at the University of Portsmouth (accelerating voltage = 15 kV) (Fig. 9).

Laser ablation (LA)-ICP-MS U-Pb isotope analyses were undertaken at the University of Portsmouth, using a New Wave 213 nm Nd:YAG laser coupled with an Agilent 7500cs quadrupole ICP-MS. Analytical protocols and instrument conditions are described in detail by Darling *et al.* (2012). Key points of the methodology are: (i) line-raster ablation (aspect ratio 1:1.5), in order to minimise time-dependent elemental fractionation; and (ii) external normalisation to the zircon standard Plesovice (Slama *et al.* 2008) using a 30 μm beam diameter. Laser beam diameters used on unknown zircons ranged from 30 to 15 μm, reflecting the scale of target domains within the crystals. Accuracy was monitored via analyses of the zircon reference materials Temora 2 and GJ-1. Eight analyses of Temora 2 (20 to 30 μm beam diameter) yield a U-Pb concordia age of 417.4 ± 3.5 Ma, and eight analyses of GJ-1 (30 μm beam diameter) yield a U-Pb concordia age of 606.6 ± 3.8 Ma: both of which are within uncertainty of the ID-TIMS reference ages for these materials (Black *et al.* 2004, Jackson *et al.* 2004).

Results

The zircons separated from sample DS1-11 are generally small (<120 μm in length). The majority of the zircons possess euhedral to sub-euhedral prismatic forms, with oscillatory or banded zonation textures as revealed by CL imaging (Fig. 8). Approximately 15 percent of grains are significantly different, and have variable habit from equant to elongate with sub-euhedral to anhedral forms. The CL textures of these grains are also variable, including sector zonation, broad banding and oscillatory zonation with spongy overgrowths. A total of 19 zircon grains were analysed by LA-ICP-MS, including a range of textural types (Table I). Three analyses were rejected due to high levels of ^{204}Pb (common Pb), which was not corrected for during data reduction.

The majority of the analyzed grains yield Silurian ages, although there is one concordant analysis with a $^{207}Pb/^{206}Pb$ age of 1284 ± 19 Ma and three slightly discordant analyses with $^{207}Pb/^{206}Pb$ ages ranging from 1725 to 1771 Ma (Table I, Fig 9a; all age uncertainties given to two standard deviations). These older grains are of the equant, anhedral group and have Th/U ratios (0.4-0.6) that are significantly lower than the Silurian grains (Th/U = 0.9 to 1.5). Ten of the prismatic, more euhedral grains with oscillatory zonation textures yield $^{206}Pb/^{238}U$ ages ranging from 416 to 436 Ma (Fig. 9b). In combination, these grains yield a concordia age of 427.3 ± 3.7 Ma. Two additional analyses yielded discordant U-Pb isotope data, and fall on a discordia line between the younger concordant population and ca. 1700 Ma. These are interpreted as mixed analyses, which is supported by the observation of variable isotopic ratios in the time resolved signals. The 427.3 ± 3.7 Ma concordia age of the younger group of prismatic zircons, with CL textures (oscillatory or fine-banded) and Th/U ratios (0.9-1.5) typical of igneous zircon, is taken as the best estimate of intrusion age of the Loch Shin Granite (Fig. 10).

RHENIUM-OSMIUM MOLYBDENITE GEOCHRONOLOGY

Samples

Four molybdenite samples were collected for rhenium-osmium (Re-Os) geochronology to constrain the timing of sulphide mineralization associated with the Loch Shin and Gruide granite intrusions. Although molybdenite mineralization was noted in several places within the Loch Shin intrusion by Gallagher & Smith (1976) only one *in-situ* quartz-molybdenite vein was observed in the field (AF33-10; NC 5614 0650; Fig. 2b). The ~1cm quartz vein hosts minor fine grained (~1mm) rosettes and disseminated molybdenite grains. No appreciable alteration selvage is present, with the exception of minor silicification, and chlorization of magmatic biotite.

Three additional samples were selected from the area around the Grudie granite and molybdenite±pyrite mineralization sufficient for geochronological analysis was only observed in the neighboring Moine rocks adjacent to the intrusion (Fig. 2b). The mineralization post-dates all ductile Moine fabrics. Molybdenite mineralization is associated with and without quartz veins and, similar to the Loch Shin granite, wallrock alteration is limited to silicification, and chloritization of biotite in the Moine rocks. Molybdenite within quartz veins is fine grained (0.5 to 1mm) and occurs as disseminations and parallel to the boundary between the quartz vein and wallrock (AF01-11; AF02-11). Molybdenite also occurs as coatings along fractures (AF36-10).

Mineral separation and analytical protocol

Molybdenite samples present in the area of the Grudie Granite were isolated using traditional methods of crushing, heavy liquids, and water floatation (Selby & Creaser, 2004). In contrast, given the minor abundant of molybdenite in the Loch Shin Granite sample (AF33-10), and to avoid losing molybdenite during crushing, the mineral separate was achieved using a room temperature HF dissolution of quartz protocol (Lawley & Selby, 2012).

The Re-Os analysis follows that outlined by Selby & Creaser (2004), which determines the Re and Os abundance of the molybdenite using isotope dilution negative thermal ionization mass spectrometry (ID-NTIMS). An aliquant of molybdenite, together with a known amount tracer solution (isotopically normal Os + ^{185}Re) are digested and equilibrated in a carius tube with 1mL 11N HCl and 3mL 15N HNO_3 for 24hrs at 220°C. Osmium is isolated and purified from the acidic solution using solvent extraction ($CHCl_3$) and micro-distillation methods. The Re is separated and purified using anion chromatography. The separated Re and Os were loaded on Ni and Pt wire filaments with $BaNO_3$ and BaOH activators, respectively, and analyzed for their isotope compositions using NTIMS via static Faraday collection. Analytical uncertainties are propagated and incorporate uncertainties related to Re and Os mass spectrometer measurements, blank abundances and isotopic compositions, spike calibrations, and reproducibility of standard Re and Os isotope values. The molybdenite analyses of this study were conducted during the same period as those of Lawley & Selby (2012). This study reported Re and Os blanks of <4 and 1 pg, respectively, with the $^{187}Os/^{188}Os$ of the blank being 0.25 ± 0.02 (n = 2). Further, Re-Os model ages determined using the ^{187}Re decay constant of 1.666×10^{-11} a^{-1} (Smoliar *et al.*, 1996) of molybdenite reference materials (NISTRM8599 = 27.6 ± 0.1 and 27.6 ± 0.1 Ma; HLP-5 = 220.0 ± 0.9 Ma), which are in good agreement with their accepted values determined at other laboratories and those previously reported at Durham University (Markey *et al.*, 1998, 2007; Porter & Selby, 2010).

Results

The four molybdenite samples from the Loch Shin (n = 1) and Gruide granites (n = 3) possess between ~1.6 and 8 ppm Re and 7.5 and 36 ppb ^{187}Os. All four molybdenite samples yield ages identical within uncertainty (Table II; Figure 10), indicating that mineralization associated with the Loch Shin and the Grudie granite intrusions occurred during the upper mid Silurian (ca. 428 – 430Ma).

FLUID INCLUSION ANALYSIS

Analytical protocols

Three molybdenite-bearing quartz veins from the Loch Shin Granite and wall rocks of the Grudie granite were studied in the Geofluids Research Laboratory at the National University of Ireland Galway. A petrographic classification scheme for the quartz-hosted fluid inclusions was developed using transmitted polarised light microscopy (Fig. 11). Microthermometric analysis was performed on doubly polished wafers (~100 mm thick) using a Linkam THMGS 600 heating freezing stage, mounted on an Olympus transmitted polarised light microscope. The instrument is equipped with a range of special long working distance objective lenses ranging up to 100x magnification. Calibration of the stage was performed using synthetic fluid inclusion standards (pure CO_2 and H_2O). Precision is ± 0.5°C at 300°C and ± 0.2°C at -56.6°C. Following procedures outlined by Shepherd *et al.* (1985), the temperature of first ice melting T_{FM}, the temperature of last ice melting T_{LM} and the temperature of homogenisation T_H were measured in quartz hosted two-phase liquid+vapour inclusions in all wafers (Fig. 12). Fluid salinities were calculated using T_{LM} and the equations of Bodnar (1993). In addition, clathrate melting temperatures recorded in three-phase (L_{H2O}+L_{CO2}+V_{CO2}) aqueous-carbonic inclusions were used with the equations of Duan *et al.*, (1996) to calculate their fluid salinities (Fig.12).

Laser Raman Microspectroscopy (LRM) of fluid inclusions was performed using a Horiba LabRam II laser Raman spectrometer. The instrument is equipped with a 600 groove mm^{-1} diffraction grating, a confocal and optical filter system, a Peltier-cooled CCD detector (255 x 1024 pixel array), and is coupled to an Olympus BX51 microscope. Fluid inclusion gas and liquid phases were analysed at room temperature using a 532nm laser focused through either a 50x or 100x microscope objectives. The spatial resolution of the 532nm laser at the sample was approximately 2μm. Individual analyses were performed for between 10 to 60 seconds over the spectral range 1100 cm^{-1} to 4200 cm^{-1}. The number of spectral accumulations per analysis typically ranged between 2 to 5 in order to maximize the signal-to-noise efficiency of the spectrometer. Calibration of the instrument was routinely performed between analyses using the Raman peak of a pure silicon standard (520.7 cm^{-1}). Spectral uncertainty associated with the generation of Raman peak positions is estimated to be ± 1.5 cm^{-1} (2σ; 0.3%) based on replicate analyses of the standard.

Fluid Inclusion Petrography

Molybdenite-bearing quartz veins were investigated from the Loch Shin Granite (one sample: AF33-10) and from the Moine wall rocks of the Grudie Granite (two samples: AF35-10 and AF02-11). The fluid inclusion petrographic study adopted the concept of fluid inclusion assemblages (FIA) described by Goldstein (2003), an approach that places fluid inclusions into assemblages interpreted to represent contemporaneous fluid trapping. Fluid inclusions (FIs) in all samples display ellipsoidal to irregular morphologies. Inclusions are commonly ~10μm in longest dimension and show low degrees of fill (F=0.7-0.95). The degree of fill [F=vol. liquid / (vol. liquid + vol. vapour)] was measured by estimating the proportions of liquid and vapour at 25°C and comparing to published reference charts (Shepherd *et al.*, 1985). Four inclusion types (*Type 1, Type 2, Type 3* and *Type 4*) have been identified hosted in vein quartz and their petrological characteristics are presented in Table III. The classification scheme is based on phase relations in fluid inclusions at room temperature. Photomicrographs of fluid inclusion assemblages from each sample are presented in Figure 11 and described below:

- *Type 1* are two-phase liquid-rich (L>V) aqueous inclusions. They are abundant in all three samples, occurring in trails and in clusters and they commonly display subrounded to irregular shapes. They range from 9 μm to 25 μm in length and their degree of fill is ~0.70 to 0.95.
- *Type 2* are monophase aqueous fluid inclusions (L only), and are present in all samples. They occur in trails alongside Type 1 FIs and range in longest dimension from 1 μm to 5 μm in length. These are interpreted as being metastable and indicate fluid trapping temperatures of < 50°C (Goldstein and Reynolds, 1994).
- *Type 3* are three-phase (L+L+V) aqueous-carbonic fluid inclusions. They are aligned within annealed fractures and occur as clusters or as isolated individuals. They exhibit subrounded to subangular morphologies that range between 4 and 17 μm in the longest dimension.

- *Type 4* are monophase (L) carbonic fluid inclusions. They are aligned within annealed fractures and also occur in clusters associated with Type 3 aqueous-carbonic inclusions. They range between 5 and 10 μm in longest dimension and possess rounded to sub-rounded morphologies. They are rare and have been observed in samples AF33-10 (Loch Shin Granite) and AF02-11 (Grudie Granite).

Fluid Inclusion Microthermometry

In sample AF33-10 from the Loch Shin Granite, T_{FM} values for Type 1 range from -50.5° to -45.5°C. This temperature interval indicates the probable presence of NaCl and $CaCl_2$ (Shepherd *et al.*, 1985). T_{LM} values are from -13.5 to -1.1°C yielding salinities ranging from ~ 1.9 to 17.3 eq. wt. % NaCl (mean 9.7 eq. wt. % NaCl). Fluid inclusions homogenise to the liquid state between 119°-170°C (Table III, Fig. 12 left plot).

T_{FM} values for Type 1 in sample AF02-11 from the Grudie Granite wall rocks range between -23° and -22.5°C corresponding to the eutectic point of the H_2O-NaCl±KCl system. T_{LM} values range from -3.60 to -0.70°C yielding salinities of ~3.7 to 6.9 eq. wt. % NaCl (mean 5.4 eq. wt. % NaCl). Homogenization to the liquid state occurs between 214° and 279°C. In sample AF35-10 T_{LM} values for Type 1 range from -4.3° to -2.2°C yielding salinities ranging from ~1.2 to 5.9 eq. wt. % NaCl (mean 4.4 eq. wt. % NaCl) Type 1 FIs homogenise to the liquid state between 151° and 244°C (Table III, Fig. 12 left plot).

Type 3 aqueous-carbonic inclusions have been identified in all three samples but only microthermometry on Grudie Granite samples (AF02-11 and AF35-10) are reported here, because of the size (<3 microns) of these inclusions in the Loch Shin sample. CO_2 homogenisation (to the liquid state, and by meniscus fading at 31.10°C) occurs between 28° and 30.9°C yielding CO_2 densities that range between 0.47 and 0.65 gm/cc. CO_2 melting temperatures range from -56.6°C (the triple point for pure CO_2) to -57.2°C, the latter indicates the presence of additional species (*e.g*. H_2S +H_2 – see LRM results). Clathrate (CO_2 5.75 HO_2) melting takes place between +5.6° and +9.9°C yielding aqueous phase salinities between ~0.2 and 8.1 eq. wt. % NaCl. Total homogenization to the liquid state occurred between 214.2° and 279.5°C in sample AF35-10, and between 262° and 308.2°C in sample AF02-11. Homogenization to the vapour phase occurred in three inclusions in sample AF02-11 at ~332.7°C (Table III, Fig. 12, left plot).

Laser Raman Microspectroscopy

Laser Raman Microspectroscopy (LRM) was used to identify the phases present in all fluid inclusion types observed in the three samples. LRM revealed the presence of CO_2, N_2 and H_2S (Fig. 13). LRM of Type 1 fluid inclusions in all samples indicates the presence of CO_2. Type 3 FIs from the Grudie granite wall rock samples have in addition to CO_2, trace amounts of H_2S and H_2. LRM of Type 4 FIs from both granites indicates that they are composed of pure CO_2 with trace amounts of H_2S.

Interpretation

The Mo-bearing veins from each of the granites contain a similar range of fluid inclusion types, *i.e*. Types 1-4. Type 1 in the Grudie Granite wall rock veins display similar fluid salinities that range between ~1 and 7 eq. wt. % NaCl. However, Type 1 from the Loch Shin Granite, display a significantly wider range of salinities *i.e*. ~2-18 eq. wt. % NaCl. This difference is coupled with T_H values for the Loch Shin sample that are generally <180°C which contrasts markedly with the range recorded for Type 1 and 3 from the Grudie Granite wall rock veins (~180°-350°C). T_H histograms (Fig. 12, left plot) for Type 1 and 3 fluid inclusions indicate a decrease in homogenization temperatures from Type 3 (~340°C) through Type 1 (~260°C) in the Grudie Granite wall rock veins to Type 1 (<180°C) fluid inclusions in the Loch Shin Granite vein. Bivariate plots of T_H and salinity show no obvious correlations, however, Type 1 inclusions from the Loch Shin Granite vein display an essentially isobaric variation in salinity (Fig 12, right plot). This low T isobaric trend displayed by the Loch Shin Type 1 inclusions is directly comparable to that displayed by high salinity fluids (Type 3) recorded in the Galway, Donegal, Newry and Leinster Granites in Ireland. Here, they are interpreted to represent basinal brines, sourced in overlying sedimentary basins, which circulated through the crystalline basement during a period of post-Caledonian crustal extension or transtension (see Conliffe and Feely, 2010 and references therein). It is arguable, therefore, that the Type 1 fluids recorded in the Loch Shin vein may post-date and be unrelated to Mo-mineralisation. Consequently P-T modelling using the fluid inclusion data is only performed for the Grudie Granite veins.

P-T Modelling

Grudie Granite wall rock veins: The molybdenite Re-Os chronometry shows that the mineralisation in both veins is contemporaneous and occurred ca. 428Ma. Accordingly, the timing of fluid trapping in AF02-11 and AF35-10 is considered to be broadly contemporaneous. Bulk fluid inclusion parameters were calculated using the LRM results in combination with the microthermometric data, using the computer programs CLATHRATES (Bakker, 1997) and FLUIDS (Bakker, 2003).

Isochores for the high and lower temperature Type 1 aqueous fluids and for the Type 3 aqueous carbonic fluids in the two vein samples are presented in the P-T diagram (Fig. 14). The field for Type 3 inclusions is defined by two isochores that reflect their range of microthermometric data. Isochores for the lower and higher temperature Type 1 aqueous fluids were constructed for salinities of ~4.5 and 5 eq.wt% NaCl matched with T_H values of ~176 and ~251°C, respectively corresponding to their range of salinities and T_H values. The veins are spatially and genetically related to the Grudie Granite which places constraints on the pressure regime active during mineralisation. Ferguson and Al-Ameen (1985) calculated pressures of 2.50±0.25kb for the aureole of the Omey Granite, Connemara which has Mo mineralisation of a similar age and setting to the Grudie Granite (Feely *et al.*, 2007). These pressure constraints are used in Figure 14 to estimate trapping temperatures for Type 3 fluids of ~340 to 410°C. Furthermore, Gallagher *et al.*, (1992) used fluid inclusion microthermometry and stable isotope data to generate a P-T model for Mo- mineralisation at the western end of the Galway Granite which yielded pressures of 1.2 to 2.0kb and a temperature range of 360 to 450°C (see

Figure 14). A higher pressure and lower temperature regime prevailed during Grudie Granite mineralisation indeed similar to that modelled for the Omey Granite (Feely *et al.*, 2007). No evidence for fluid immiscibility was recorded in Type 1 inclusions and therefore they could have been trapped anywhere along their respective isochores. Type 1 fluids are considered to be meteoric and trapped after and at lower pressures than the earlier magmatic aqueous carbonic Type 3 inclusions considered to be responsible for the Mo-mineralisation. The P-T history of fluids in the Grudie Granite wall rock veins may have followed the path shown in Figure 14 (black arrow).

DISCUSSION

The relative and absolute ages of plutonism, mineralisation and deformation

The U-Pb zircon and Re-Os molybdenite ages for the Loch Shin Granite and sulphide mineralization associated with both plutons are all coincident and overlap almost exactly within error (Fig. 10). These ages therefore confirm the geological observations which suggest that the plutons and associated mineralisation are contemporaneous and genetically related. The Loch Shin-Grudie granite ages overlap within error with the U-Pb zircon (TIMS) age of 425 ± 1.5 Ma reported by Kocks *et al.* (2013) for the central granodiorite of the Rogart pluton (Fig. 1a) which was, according to these authors also emplaced contemporaneously with dextral movements along the Strath Fleet Fault, the along strike southeastern continuation of the Loch Shin Fault and the LSL (Fig. 1a).

The field and thin section observations suggest that the Loch Shin and Grudie granites are petrologically similar – as suggested by previous authors (e.g. Gallagher & Smith 1976). Both plutons post-date the ductile deformation fabrics in the surrounding Moine and Lewisian rocks, including the main Scandian-age D2 structures. Both plutons are associated with a variety of ore mineralization, including molybdenite and other base metal sulphides, and both are post-dated by the effects of brittle deformation consistent with dextral transtensional movements along the WNW-ESE-trending Loch Shin Fault. Unsurprisingly the intensity of this brittle overprint is greater in the Loch Shin pluton which lies closer to the main fault trace.

The relative ages of the brittle faulting and mineralization are more complex. Field and thin section observations of fracture-hosted sulphides (pyrite, chalcopyrite) show that at least some of the base metal mineralization is contemporaneous with the brittle deformation. This lends support to the long postulated proposal that the dextral movements along NW-SE faults such as the Loch Shin, Strath Fleet and Dornoch Firth fault systems are contemporaneous with, and antithetic to the regional sinistral movements along the Great Glen Fault Zone ca 425 Ma (Johnson & Frost 1977; Watson 1984; Stewart *et al.* 2001). It also strengthens the arguments made by Dewey & Strachan (2003) and Kocks *et al.* (2013) that the switch from regional sinistral transpression with thrusting to transtension with regional strike slip faulting occurred at this time.

However, many brittle fractures also cross-cut mineral veins. Furthermore, the Type 1 fluid inclusions seen as Tuttle lamellae in the Loch Shin granite are clearly distinct from the fluid inclusion sets seen in the Grudie granite. Their presence points to a somewhat later, near surface phase of fluid flow associated with brittle dextral movements along the Loch Shin-Strath Fleet Fault system. Given this specific association, it seems most likely that at least some dextral faulting and fluid flow occurred over a protracted period into the Devonian (?Emsian, ca 410 Ma) where it was associated with basin development and the very final stages of late Caledonian strike-slip faulting/transtension (cf. Dewey & Strachan 2003).

Pluton relationships at depth and the magnitude of dextral strike-slip faulting

The very poor levels of exposure in the Loch Shin-Lairg region make it difficult to ascertain how the various plutonic bodies in this area may be related in 3 dimensions. Gravity modelling by Hipkin & Hussain (1983) has ruled out the possibility that the large regional gravity low seemingly centred on the surface outcrop of the Grudie pluton (Fig. 1b) is due to the presence of a very large pluton at depth. More recent work by Leslie *et al.* (2010) suggests that the low occurs mainly due to the presence of a thick thrust culmination of Moine rocks (the Cassley Culmination, Fig. 2a) sitting structurally above and to the SE of the Assynt Culmination. Nevertheless, their gravity models suggest the presence of a shallowly buried pluton with horizontal dimensions of 7 x 11 km, with an average thickness of up to 3 km (see Leslie *et al.* 2010, fig. 10). Even allowing for the significant errors in these calculations, this does indicate that the granites exposed in the Loch Shin-Lairg region (including the Grudie, Loch Shin, Claonel bodies) are likely to be underlain by a larger, possibly composite plutonic body located mainly to the SW of

Loch Shin (Fig. 15a). It is tempting to suggest that this buried granite and the similarly composite Rogart body are part of a single pluton offset by dextral strike-slip faulting. However, this would require right lateral displacement of at least 10 km which seems at odds with other regional evidence. For example, the observed offsets of regional markers such as the nearby Loch Shin Lewisian inlier (Fig 2a) suggest displacements of no more than a few hundred metres, as does the observation that the Loch Shin Fault does not appear to continue very far to the NW beyond the end of Loch Shin (Leslie et al. 2010). It seems more likely therefore that the two plutons are separate, composite bodies located either side of the Loch Shin-Strath Fleet fault system in a manner rather similar to other Caledonian plutons that are associated with regional strike-slip fault zones in NW Scotland, most notably the Great Glen Fault (e.g. Hutton 1988b; Jacques & Reavy 1994; Stewart *et al.* 2001).

Implications for the nature and significance of the Loch Shin Line

The present study lends support to the suggestion of Watson (1984) that the NW-SE trending Loch Shin Line (LSL) is associated with an anomalous zone of broadly contemporaneous mantle-derived appinites, granites (Rogart, Grudie, Loch Shin and many smaller satellite bodies) intruded ca. 425-428 Ma. These are postdated by slightly younger (perhaps as young as ca 410 Ma) brittle dextral faulting in the Moine Nappe SE of the Moine Thrust (Loch Shin-Strath Fleet and Dornoch Firth faults, Fig. 1b). Watson (1984) suggested that the LSL corresponds to the location of a Precambrian shear zone in the Lewisian autochthon underlying the Moine Nappe which acted as a deep crustal channelway controlling the ascent of magmas and mineralization during the later stages of the Caledonian orogeny (see also the leaky lower crustal fault block model of Jacques & Reavy 1994). The most obvious candidate structure seen in the Lewisian Complex west of the Moine Thrust Zone is the steeply S-dipping Laxford Front, the major shear zone that separates the Rhiconich and Assynt terranes; this lies almost parallel to and along strike from the trace of the LSL (Figs 1, 15b).

Constraints on regional exhumation rates at the end of the Caledonian orogeny

The PT estimates derived from the fluid inclusion study reported here (Fig. 14) can be compared with those for peak metamorphism in the central part of the foreland-propagating Scandian thrust wedge in Sutherland in order to provide constraints on the rate of regional exhumation. Integrated metamorphic and isotopic studies and thermal modelling suggest that peak metamorphic conditions in the vicinity of the Naver Thrust of ca. 650°C and 5.5 kbar (Friend *et al.* (2000) were attained at c. 440-435 Ma (Johnson & Strachan 2006; Thigpen *et al.* 2013). In contrast, this study has established temperature-pressure conditions at the time (ca. 425 Ma) of Grudie Granite mineralisation of c. 375°C and 2.5 kb. The contrasting pressure estimates suggest that around 10 km thickness of crust was removed in c. 10-15 myr, easily achieved at an erosion rate of less than or equal to 1mm $^{a-1}$. Essentially the same erosion rate was derived by Johnson & Strachan (2006) from consideration of isotopic data and the likely (Emsian) age of the oldest Old Red Sandstone strata to rest unconformably on the Moine rocks.

The regional significance of Caledonian molybdenite mineralization

Intrusion-related molydenite mineralization is documented throughout the Scottish and Irish Caledonian-Appalachian Orogen (Figure 1a inset). The broad timing and fluid characteristics of intrusion-related Mo-mineralisation in the Loch Shin and Grudie Granite veins (ca. 428 Ma) is temporally similar to that of the Ballachulish and Kilmelford igneous complexes (ca. 433-426 Ma; Conliffe *et al.*, 2010), pre-dates that of the Etive Igneous Complex (ca. 415 Ma; Porter and Selby, 2010), Shap granite (ca. 405 Ma; Selby *et al.*, 2008) and the earliest granite related Mo-mineralisation in the Irish sector of the Caledonian-Appalachian Orogen (ca. 423Ma, Feely *et al.*, 2010). Fluid inclusion data for these systems indicate that Mo-mineralization is ultimately associated with aqueous-carbonic fluids, which has also been shown to be common among Cu+Mo mineralization associated with late Caledonian magmatism (Kay 1985; Gallagher *et al.* 1992; Feely *et al.* 2007; Selby *et al.* 2008; this study; Feely & Selby, unpub data; see Appendix).

Gold mineralisation in Dalradian metamorphic rocks at Curraghinalt, Northern Ireland (Parnell *et al.* 2000; Rice *et al.*, 2012) and Tyndrum, Scotland (Pattrick *et al.* 1988; Curtis *et al.* 1993) has also been linked to aqueous-carbonic magmatic fluids that may have been derived from an underlying Caledonian intrusive. Although CO_2 has only an indirect role on gold mineralization (Lowenstern 2001), it may play a significant role in magmatic fluid exsolution and evolution, and may lead to concentrations of Au, Cu and Mo into the vapour phase (Heinrich *et al.* 1999; Ulrich *et al.* 2001). As such, intrusion-related Mo (+Cu) mineralization may warrant attention during future mineral exploration, particularly for porphyry Cu–Mo-Au mineralization and additionally for structurally-controlled Au-mineralisation distal from the intrusion. In this regard combined fluid inclusion data, U-Pb and Re-Os geochronometry have shown that prolonged granite related molybdenite mineralisation in the Connemara region was accompanied by aqueous-carbonic fluids in the Omey Granite at ca. 423 Ma and later in the Galway Granite at ca. 410Ma (Murvey), ca. 407Ma (Mace Head) and ca. 380Ma (Costelloe; Feely *et al.*, 2007, 2010). Moreover, the earliest granite related Mo-mineralisation of the Omey Granite was also initiated while major orogen parallel structures, *e.g*. Great Glen and Southern Upland Fault systems (Dewey and Strachan, 2003) were active.

CONCLUSIONS

Using detailed field observations, microstructural studies, U-Pb zircon and Re-Os molybdenite geochronology and fluid inclusion analyses, we have shown that a suite of mid-Silurian (ca. 425-430 Ma) granite plutons (Grudie, Loch Shin, Rogart and many smaller associated bodies) are contemporaneous with base metal sulphide mineralization, including molybdenite. Synchronous to slightly younger (ca. 427-410Ma) brittle dextral strike slip faulting along the WNW-ESE Loch Shin-Strath Fleet Fault System was antithetic to regional sinistral strike-slip movements along the NE-SW trending Great Glen Fault (Fig. 15a). More generally, the associated plutonism, mineralization and strike-slip faulting confirms the transition from regional-scale transpression to transtension during the mid-Silurian to early Devonian in NW Scotland as postulated by Dewey & Strachan (2003).

Our findings also lend support to the existence of the NW-SE trending Loch Shin Line and to the hypothesis of Watson (1984) that it has acted as a deep crustal channelway controlling the ascent and emplacement of Silurian granitic and appinitic magmas into the overlying Moine Nappe (Fig. 15b). It seems very likely that this deep structure corresponds to the southeastern continuation of the Precambrian-age Laxford Front shear zone in the buried Lewisian autochthon. This further illustrates how pre-existing crustal structures can be persistently reactivated even when buried beneath much younger thrust nappes and influence directly the migration and emplacement of hydrous mineralizing fluids and magmas (e.g. Jacques & Reavy 1994; Richards 2013).

Acknowledgements

To be added

References

Alsop, G.I., Cheer, D.C., Strachan, R.A., Krabbendam, M., Kinney, P.D., Holdsworth, R.E. & Leslie, A.G. 2010. Progressive fold and fabric evolution associated with regional strain gradients: A case study from across a Scandian ductile thrust nappe, Scottish Caledonides. In: Law, R.D., Butler, R.W.H., Holdsworth, R.E., Krabbendam, M. & Strachan, R.A.. (eds) *Continental Tectonics and Mountain Building: The Legacy of Peach and Horne,* Geological Society, London, Special Publication, 335 255-276. DOI: 10.1144/SP335.12

Bakker, R.J., 1997. Clathrates: computer programs to calculate fluid inclusion V-X properties using clathrate melting temperatures. *Computers & Geosciences*, **23**, 1-18.

Bakker, R.J., 2003. Package FLUIDS 1. Computer programs for analysis of fluid inclusion data and for modelling bulk fluid properties. *Chemical Geology*, **194**, 3-23.

Barr, D., Holdsworth, R.E. & Roberts, A M. 1986. Caledonian ductile thrusting within a Precambrian metamorphic complex: the Moine of N.W. Scotland. *Bulletin of the Geological Society of America,* 97, 754-64.

Black, L.P., Kamo, S.L., *et al.* 2004. Improved 206Pb/238U microprobe geochronology by the monitoring of a trace-element-related matrix effect; SHRIMP, ID–TIMS, ELA–ICP–MS and oxygen isotope documentation for a series of zircon standards. *Chemical Geology*, **205**, 115–140, doi: 10.1016/j.chemgeo.2004.01.003.

Bodnar, R.J., 1993. Revised equation and table for determining the freezing point depression of H_2O–NaCl solutions. *Geochimica Cosmochimica Acta*, **57**, 683–684.

Butler, R.W.H. & Coward, M.P. 1984. Geological constraints, structural evolution and the deep geology of the NW Scottish Caledonides. *Tectonics,* **3,** 347-365.

Conliffe, J., Selby, D., Porter, S.J. & Feely, M., 2010. Re-Os molybdenite dates from the Ballachulish and Kilmelford Igneous complexes (Scottish Highlands) et al. 2010.: age contraints for late Caledonian magmatism. *Journal of the Geological Society, London,* **167,** 297-302.

Curtis, S.F., Pattrick, R.A.D., Jenkin, G.R.T., Fallick, A.E., Boyce, A.J. & Treagus, J.E., 1993. Fluid inclusion and stable isotope study of fault related mineralization in Tyndrum area, Scotland. *Transactions of the Institute of Mining and Metallurgy* (Section B: Applied Earth Science), **102**, 39-47.

Darling, J.R., Storey, C.D. & Engi, M. 2012. Allanite U–Th–Pb geochronology by laser ablation ICPMS. *Chemical Geology*, **292-293**, 103–115, doi: 10.1016/j.chemgeo.2011.11.012.

Dewey, J. F. and Strachan, R. A. 2003. Changing Silurian-Devonian relative plate motion in the Caledonides: sinistral transpression to sinistral transtension. *Journal of Geological Society (London*), **160**, 219–229.

Dewey, J.F., Hempton, M.R., Kidd, W.S.F., Saroglu, F. & Şengör, A.M.C. 1986. Shortening of continental lithosphere: the neotectonics of Eastern Anatolia – a young collision zone. *In*: Coward, M.P. & Ries, A.C. (eds) *Collision Tectonics*, Geological Society of London, Special Publication, **19**, 3-36.

Duan, Z., Moller, N. and Weare, J.H., 1996. A general equation of state for supercritical fluid mixtures and molecular dynamics simulation of mixture PVTX properties. *Geochimica Cosmochimica Acta*, **60**, 1209–1216

Elliott, D. & Johnson, M.R.W. 1980. Structural evolution in the northern part of the Moine thrust belt, NW Scotland. *Transactions of the Royal Society of Edinburgh: Earth Sciences,* **71,** 69-96.

Feely, M., Selby, D., Conliffe, J., and Judge, M., 2007. Re–Os geochronology and fluid inclusion microthermometry of molybdenite mineralisation in the late-Caledonian Omey granite, western Ireland. *Trans. Inst. Min. Metall. B, Appl. Earth Sci*., 2007, **116B**, 143–149.

Feely, M., Selby, D., Hunt, J. & Conliffe, J. (2010). Long-lived granite-related molybdenite mineralisation at Connemara, western Irish Caledonides. *Geological Magazine. 147 (6), pp. 886-894*

Ferguson, C.C., Al-Ameen, S.I., (1985) C.C. Muscovite breakdown and corundum growth at anomalously low fH_2O: a study of contact metamorphism and convective fluid movement around the Omey granite, Connemara, western Ireland, Min. Mag., 1985, 49, 505-515.

Fowler, M.B. 1992. Elemental and O-Sr-Nd isotope geochemistry of the Glen Dessary Syenite, NW Scotland. *Journal of the Geological Society of London*, **149**, 209-220.

Fowler, M.B. & Henney, P.J. 1996. Mixed Caledonian appinite magmas: implications for lamprophyric fractionation and high Ba-Sr granite genesis. *Contributions to Mineralogy and Petrology*, **126**, 199-215.

Fowler, M.B., Henney, P.J., Darbyshire, D.P.F. & Greenwood, P.B. 2001. Petrogenesis of high Ba—Sr granites: the Rogart pluton, Sutherland. *Journal of the Geological Society, London,* **158,** 521-534.

Fowler, M.B., Kocks, H., Darbyshire, D.P.F. & Greenwood, P.B. 2008. Petrogenesis of high Ba—Sr granitoids from the Northern Highland Terrane of the British Caledonian Province. *Lithos*, **105**, 129-148.

Friend, C.R.L., Jones, K.A. & Burns, I.M. 2000. New high pressure event in the Moine Supergroup, northern Scotland: implications for Taconic (early Caledonian) crustal evolution. *Geology*, 28, 543-546.

Gallagher, M.J. & Smith, R.T. 1975 *Molybdenite mineralisation in Precambrian rocks, near Lairg, Scotland.* Institute of Geological Sciences, 86pp.

Gallagher, V., Feely, M., Hoegelsberger, H., Jenkin, G. R. T. and Fallick, A. E., 1992. Geological, fluid inclusion and stable isotope studies of Mo mineralization, Galway Granite, Ireland. *Mineralium Deposita,* **27,** 314– 325.

Goldstein, R.H. & Reynolds, T.J., 1994. Systematics of fluid inclusions in diagenetic minerals. *SEPM Short Course*, **31**, 199pp.

Goldstein, R.H., 2003. Re-equilibrium of fluid inclusions. *Mineralogical Association of Canada, Short Course Series*, 9–53.

Goodenough, K.M., Millar, I.L., Strachan, R.A., Krabbendam, M. & Evans, J.A. 2011. Timing of regional deformation and development of the Moine Thrust Zone in the Scottish Caledonides: constraints from the U-Pb geochronology of alkaline intrusions. *Journal of the Geological Society, London,* **168**, 99-114.

Heinrich C. A., Gunther D., Audetat A., Ulrich T. and Frischknecht R., 1999. Metal fractionation between magmatic brine and vapor, determined by microanalysis of fluid inclusions. *Geology*, **27,** 755–758.

Hipkin, R.G. & Hussain, A., 1983. Regional gravity anomalies: Northern Britain, Institute of Geological Sciences, Reports, 82/10.

Holdsworth, R.E. & Grant, C.J. 1990. Convergence - related 'dynamic spreading' in a mid-crustal ductile thrust zone: a possible orogenic wedge model. *In:* Knipe, R.J. & Rutter, E.H. (eds.) *Deformation Mechanisms, Rheology and Tectonics.* Special Publication of the Geological Society, London, 54, 491-500.

Holdsworth, R.E. & Strachan, R.A 1988. The structural age and possible origin of the Vagastie Bridge granite and associated intrusions, Central Sutherland. *Geological Magazine,* 125,.613-20.

Holdsworth, R.E. Strachan, R.A. and Harris, A.L. 1994. The Moine Supergroup. *In:* Gibbons, W. and Harris, A.L. (eds) *A Revised Correlation of Precambrian Rocks in the British Isles*. Geological Society of London, Special Report, No. 22,], 23-32.

Holdsworth, R.E., Butler, C.A. & Roberts, A.M. 1997. The recognition of reactivation during continental deformation. *Journal of the Geological Society, London,* 154, 73-78.

Holdsworth, R.E., Stewart, M., Imber, J. & Strachan, R.A. 2001. The structure and rheological evolution of reactivated continental fault zones: a review and case study. *In:* Miller, J.A., Holdsworth, R.E., Buick, I.S. & Hand, M. (eds) *Continental Reactivation* and *Reworking.* Special Publication of the Geological Society, London, 184, 115-137.

Hutton, D.H.W. 1988a. Granite emplacement mechanisms and tectonic controls: inferences from deformation studies. *Transactions of the Royal Society of Edinburgh: Earth Sciences*, Vol. 79, 245-255.

Hutton, D.H.W. 1988b. Igneous emplacement in a shear zone termination: the biotite granite at Strontian, Scotland. *Geological Society of America Bulletin,* **100,** 1392-1399.

Hutton, D.H.W. & McErlean, M.A. 1991. Silurian and Early Devonian sinistral deformation of the Ratagain Granite, Scotland: constraints on the age of Caledonian movements on the Great Glen Fault System. *Journal of the Geological Society of London,* **148,** 1-4.

Jackson, S.E., Pearson, N.J., Griffin, W.L. & Belousova, E.A. 2004. The application of laser ablation-inductively coupled plasma-mass spectrometry to in situ U–Pb zircon geochronology. *Chemical Geology*, **211**, 47–69, doi: 10.1016/j.chemgeo.2004.06.017.

Jacques, J.M. & Reavy, R.J. 1994. Caledonian plutonism and major lineaments in the SW Scottish Highlands. *Journal of the Geological Society, London,* **151,** 955-969.

Johnson, M.R.W. & Frost, R.T.C. 1977. Fault and lineament pattern in the Southern

Highlands of Scotland. *Geologie en Mijnbouw,* **56,** 287-294.

Johnson, M.R.W. & Strachan, R.A. 2006. A discussion of possible heat sources during nappe stacking: the origin of Barrovian metamorphism within the Caledonian thrust sheets of NW Scotland. *Journal of the Geological Society, London,* **163**, 579-582.

Kay, E.A. 1985. *Hydrothermal Mineralization and Alteration of the Lagalochan Au-Cu-Mo Prospect, W. Scotland.* Unpublished PhD thesis, University of London.

Kinny, P.D., Friend, C.R.L., Strachan, R.A., Watt, G.R. & Burns, I.M. 1999. U-Pb geochronology of regional migmatites in East Sutherland, Scotland: evidence for crustal melting during the Caledonian Orogeny. *Journal of the Geological Society, London*, **156**, 1143-1152.

Kinny, P.D., Strachan, R.A., Rogers, G.R., Friend, C.R.L. & Kocks, H. 2003. U—Pb geochronology of deformed meta-granites in central Sutherland, Scotland: evidence for widespread Silurian metamorphism and ductile deformation of the Moine Supergroup during the Caledonian orogeny. *Journal of the Geological Society, London*, **160**, 259-269.

Kocks, H., Strachan, R.A. & Evans, J.A. 2006. Heterogeneous reworking of Grampian metamorphic complexes during Scandian thrusting in the Scottish Caledonides: insights from the structural setting and U-Pb geochronology of the Strath Halladale Granite. *Journal of the Geological Society, London*, **163**, 525-538.

Kocks, H., Strachan, R.A., Evans, J.A. & Fowler, M.B. 2013. Contrasting magma emplacement mechanisms within the Rogart igneous complex, NW Scotland, record the switch from regional contraction to strike-slip during the Caledonian orogeny. *Geological Magazine*, **151**, 899-915.

Lawley, C.J.M., and Selby, D. 2012. Re-Os Geochronology of Quartz Enclosed Ultra-fine Molybdenite: Implications for Ore Geochronology, *Economic Geology, v. 107, 1499-1506.*

Leslie, A.G., Krabbendam, M., Kimbell, G.S. & Strachan, R.A. 2010. Regional-scale lateral variation and linkage in ductile thrust architecture: the Oykell Transverse Zone, and mullions, in the Moine Nappe, NW Scotland. *In*: Law, R.D., Butler, R./W.H., Holdsworth, R.E., Krabbendam, M. & Strachan, R.A. (eds) *Continental Tectonics and Mountain Building: The Legacy of Peach and Horne*. Geological Society, London, Special Publications, **335**, 359-381.

Lowenstern, J.B., 2001, Carbon dioxide in magmas and implications for hydrothermal systems: *Mineralium Deposita*, **36,** 490-450.

O'Driscoll, E.S.T. 1986. Observations of the lineament - ore relation. Philosophical Transactions of the Royal Society, London, A317, 195-218.

Pernell, J., Earls, G., Wilkinson, J. J., Hutton, D. H. W., Boyce, A. J., Fallick, A. E., Ellam, R. M., Gleeson, S. A., Moles, N. R., Carey, P. F., & Legg, I. 2000. Regional Fluid Flow and Gold Mineralization in the Dalradian of the Sperrin Mountains, Northern Ireland: *Economic Geology*, **95,** 1389-1416.

Paterson, S.R. & Tobisch, O.T. 1988. Using pluton ages to date regional deformations; problems with commonly used criteria. *Geology*, **16**, 1108-1111.

Pattrick, R.A.D., Boyce, A. J. & MacIntyre, R.M. 1988. Gold-silver vein mineralization at Tyndrum, Scotland. *Mineralogy and Petrology*, **38,** 61-76.

Peacock, J.D. 1975. Slide rocks in the <oine of the Loch Shin area, northern Scotland. Bulletin of the Institute of Geological Sciences, 49, 23-30.

Porter, S.J., Selby, D. 2010. Rhenium-Osmium (Re-Os) molybdenite systematics and geochronology of the Cruchan Granite skarn mineralization, Etive Complex: implications for emplacement chronology. *Scottish Journal of Geology*, 46, (1), 17-21.

Read, H.H., Ross, G., Phemister, J. & Lee, G.W. 1925. *The geology of the country around Golspie, Sutherlandshire*. Memoir of the Geological Survey, Scotland. HMSO.

Read, H. H., Phemister, J. & Ross, G. 1926. T*he Geology of Strath Oykell and Lower Loch Shin.* Memoir of the Geological Survey, Scotland, HMSO.

Rice, C.M. & Cope, M.J. 1973. *The ore mineralogy of some rocks from the Loch Shin area.* Institute of Geological Sciences, Mineralogy Unit Report, 125, 7pp.

Rice C. M., Mark D. F., Selby D., Hill N. J. 2012. Dating vein-hosted Au deposits in the Caledonides of N. Britain. Mineral Deposit Studies Groups meeting abstracts. *Transactions of the Institute of Mining and Metallurgy Section B: Applied Earth Science,* **121,**199–200.

Richards, J.P. 2013 Giant ore deposits formed by optimal alignments and combinations of geological processes. *Nature Geosciences*, 1-6, doi. 10.1038/NGEO1920.

Rosenberg, C.L. 2004. Shear zones and magma ascent: a model based on a review of the Tertiary magmatism in the Alps. *Tectonics*, **23**, 1-21.

Schofield, D. & D'Lemos, R.S. 1998. Relationships between syn-tectonic granite fabrics and regional PTtd paths: an example from the Gander-Avalon boundary of NE Newfoundland. *Journal of Structural Geology*, **20**, 459-471.

Slama, J., Kosler, J., *et al.* 2008. Plesovice zircon - A new natural reference material for U-Pb and Hf isotopic microanalysis. *Chemical Geology*, **249**, 1–35, doi:

10.1016/j.chemgeo.2007.11.005.

Selby, D., and Creaser, R.A., 2004. Macroscale NTIMS and microscale LA-MC-ICP-MS Re-Os isotopic analysis of molybdenite: Testing spatial restrictions for reliable Re-Os age determinations, and implications for the decoupling of Re and Os within molybdenite. *Geochimica et Cosmochimica Acta,* v. 68, p. 3897-3908.

Shepherd, T.J., Rankin, A.H. and Alderton, D.H.M., 1985. A practical guide to fluid inclusion studies. Glasgow and London, Blackie, Glasgow, 239pp.

Smoliar, M. I., R. J. Walker, *et al.* (1996). "Re-Os isotope constraints on the age of Group IIA, IIIA, IVA, and IVB iron meteorites." Science 271: 1099-1102.

Soper, N.J. 1963. The structure of the Rogart igneous complex, Sutherland. *Quarterly Journal of the Geological Society of London*, 119, 445-478.

Soper, N.J. and Brown, P.E. 1971. Relationship between metamorphism and migmatisation in the northern part of the Moine nappe. *Scottish Journal of Geology*, Vol. 7, 305-325.

Soper, N.J., Strachan, R.A., Holdsworth, R.E., Gayer, R.A. & Greiling, R.O. 1992. Sinistral transpression and the Silurian closure of Iapetus. *Journal of the Geological Society, London,* 149, 871-880.

Stewart, M., Strachan, R.A., Martin, M.W. & Holdsworth, R.E. 2001. Constraints on early sinistral displacements along the Great Glen Fault Zone, Scotland: structural setting, U-Pb geochronology and emplacement of the syn-tectonic Clunes tonalite. *Journal of the Geological Society, London,* 158, 821-830.

Strachan, R.A. & Holdsworth, R.E. 1988. Basement - cover relationships and structure within the Moine rocks of central and southeast Sutherland. *Journal of the Geological Society, London,* 145, 23-36.

Strachan, R.A., Holdsworth, R.E., Krabbendam, M. & Alsop, G.I. 2010. The Moine Supergroup of NW Scotland: insights into the analysis of polyorogenic supracrustal sequences. In: Law, R.D., Butler, R.W.H., Holdsworth, R.E., Krabbendam, M. & Strachan, R.A. (eds) *Continental Tectonics and Mountain Building: The Legacy of Peach and Horne,* Geological Society, London, Special Publication, 335, 233-254. DOI: 10.1144/SP335.11

Sutton, J. & Watson, J.V. 1986. Architecture of the continental lithosphere. Philosophical Transactions of the Royal Society, London, A317, 5-12.

Thigpen, J.R., Law, R.D., Loehn, C.L., Strachan, R. A., Tracy, R.J., Lloyd, G.E., Roth, B.L. & Brown, S.J. (2013), Thermal structure and tectonic evolution of the Scandian orogenic wedge, Scottish Caledonides: integrating geothermometry, deformation temperatures and conceptual kinematic-thermal models. *Journal of Metamorphic Geology*, **31**, 813–842. doi: 10.1111/jmg.12046.

Torsvik, T.H., Smethurst, M.A., Meert, J.G.,Van der Voo, R., McKerrow, W.S., Brasier, M.D., Sturt, B.A. & Walderhaug. H.J., 1996. Continental break-up and collision in the Neoproterozoic and Palaeozoic:A tale of Baltica and Laurentia. *Earth Science Reviews*, **40**, 229-258.

Ulrich, T., Gunther, D., and Heinrich, C.A. 2001. The evolution of a porphyry Cu-Au deposit, based on LA-ICPMS analysis of fluid inclusions: Bajo de la Alumbrera, Argentina. *Economic Geology*, **96**, 1743–1774.

Watson, J.V. 1984. The ending of the Caledonian Orogeny in Scotland. *Journal of the Geological Society of London,* **141,** 193-214.

Figure captions

Figure 1a) Regional geology map of the northern Scottish Highlands. Inset map shows the relative positions of Laurentia, Baltica, Avalonia and Gondwana following the closure of the Iapetus Ocean (Caledonide-Appalachian belt in black). Abbreviations as follows: A = Assynt; DFF = Dornoch Firth Fault; GGF = Great Glen Fault; LCM = Loch Coire Migmatite complex; LSSFF = Loch Shin - Strath Fleet Fault ; MF = Moray Firth; MT = Moine Thrust; NT = Naver Thrust; ORS = Old Red Sandstone; R = Rogart igneous complex.

b) Gravity map of the Lairg-Loch Shin area, with locations of appinnitic intrusions (Achnuie hybrids), Laxford front and surface trace of Loch Shin Line shown (after Watson 1984 and Leslie *et al.* 2010).

Figure 2a) Overview geological map of the Loch Shin area after Strachan and Holdsworth (1988) & Leslie *et al.* (2010). Box shows location of map shown in Figure 2b. G= Grudie, C = Claonel, LS = Loch Shin granites. L = Lairg; LSF = Loch Shin Fault; AS = Aird of Shin. **b)** Simplified version of geology in the Loch Shin – Grudie area (after Gallagher & Smith 1976). Geochronology sample locations are shown. GB = Grudie Burn; CCB = Cnoc na Cloich-bhuaile; MG = Meall a'Ghruididh; AC = Allt a'Chlaonaidh.

Figure 3) The country rocks, Loch Shin granite and associated veins viewed in the field and thin section. **a)** Oblique view looking down onto undeformed granite pegmatite vein (077/55 NNW) cutting ACW of compositional banding in Moine psammites (100 metres to the SE of the Loch Shin granite (NC 5639 0613). Arrow shows inferred direction of vein opening based on offsets of thin semipelite layer. **b)** Thin section of undeformed granite pegmatite vein shown in (a) cross-cutting S0-S1-S2 fabric in Moine psammites (dashed yellow line). View in crossed polars, with igneous contact shown in red. **c)** Plan view in the field (NC 5631 0650) and **d)** in thin section (crossed polars) of typical undeformed Loch Shin granite (NC 5635 0631). **e)** Close-up plan view of irregular quartz-pyrite veins cutting Loch Shin granite (NC 5631 0650). **f)** Cross-section view of large NW-SE-trending quartz-galena veins (107/85N) cutting Loch Shin granite (NC 5630 0659).

Figure 4) Equal area stereoplots of structural data collected from the Loch Shin shore section. **a)** Ductile foliation (Sn/S2; great circles) and L2 mineral lineations (dots). **b)** Granite veins (red, great circles) and quartz veins (green, great circles) and lineation on quartz vein (dot). **c)** Steep faults (great circles) and slickenlines (dots). **d)** Shallow faults (great circles) and slickenlines (dots). **e)** Box fold hinges (dots) and axial surfaces (great circles). **f)** Stress inversion analysis and Mohr plot of combined fault slickenline data with weighting added to include fault sizes. LSF = inferred local orientation of Loch Shin Fault.

Figure 5) Brittle structures cutting the Loch Shin granite and its Moine country rocks. **a)** Plan view of NE-SW sinistral fault offsetting granite and quartz vein (NC 5635 0631). **b)** Plan view of NW-SE dextral fault offsetting granite pegmatite vein in Moine psammites (NC 5639 0613). **c)** Oblique sectional view of long NW-SE trending dextral fault scarp in Loch Shin granite; inset shows sub-horizontal orientation of slickenlines on fault surface consistent with strike-slip fault movement (NC 5631 0650). **d)** NE-SW sinistral fault offsetting and being offset by NNW-SSE dextral faults in Loch Shin granite (NC 5635 0631). **e)** Shallowly NW-dipping flats and shorter SE-dipping ramps ('r') in exposed small displacement, top-to-the-NW faults; inset shows plan view of corrugated, lineated fault surface with NW-SE slickenlines (NC 5635 0632). **f)** Plan view of steeply plunging conjugate box folds detaching along sub-vertical NE-SW sinistral fault in Moine psammites (NC 5638 0621).

Figure 6) Thin sections of brittle structures and mineralization cutting the Loch Shin granite and its country rocks. **a)** Small offset (<0.5mm) domino style reverse (top-to-the-NW) shear fractures (arrowed) cutting Loch Shin granite viewed in ppl (NC 5635 0632). **b)** Typical zone of cataclasis cross cutting Loch Shin Granite viewed in crossed polars (NC 5635 0632). **c)** Irregular region of quartz iron oxide-ilmenite (black) -pyrite (black, Py) –fluorite (Fl) mineralization in Moine psammites immediately to the northwest of the Loch Shin granite viewed in ppl (NC 5625 0666). **d)** Multiple sets of fluid inclusions following healed microcracks/Tuttle lamellae in quartz from the Loch Shin granite viewed in ppl (NC 5635 0632). **e)** Microfactures lined with sericite where they cross-cut feldspar (Fsp) passing laterally into healed microcracks/Tuttle lamellae in quartz (Qtz), in granite pegmatite vein, viewed in crossed polars (NC 5639 0613). **f)** Late zeolite vein (Z) cutting brecciated Moine psammite viewed in cross-polars (NC 5625 0666).

Figure 7) Field and thin section views of the Grudie granite. **a)** Plan view of typical unfoliated Grudie granite with large pink K-feldspar and grey quartz phenocrysts/xenocrysts (NC 5268 0450). **b)** Oblique section view of slickenlined joints with chlorite and epidote mineralization (NC 5267 0444). **c)** Thin section of typical K-feldspar (in extinction) and **d)** polycrystalline quartz xenocryst/phenocrysts within Grudie granite (NC 5310 0427).

Figure 8) Plot of the U-Pb zircon and Re-Os molybdenite dates including 2 sigma uncertainty with decay constant uncertainty for the Loch Shin and Gruide granites. Also given is the weighted average for the Re-Os molybdenite dates for the Gruide granite. For sample locations, see Figure 2.

Figure 9) Cathodoluminescence images and SHRIMP II analysis positions for representative grains from grains selected for geochronology from the Loch Shin Granite sample. Also shown are the grain numbers, and 207Pb/206Pb ages for each analysis pit (uncertainties are two standard deviations; percentage discordance shown in brackets).

Figure 10 a, b) Zircon U-Pb concordia plots from the Loch Shin granite.

Figure 11) Photographs of fluid inclusions (FI) trails from samples AF33-10 – Loch Shin Granite (**a,b**); AF35-10 (**c,d**) and AF02-10 (**e,f**) both from Gruide Granite. Scale bar = 50 μm.

Figure 12) Histogram of TH values (a) and bivariate plot of TH vs. salinity (b) for Type 1 and Type 3 inclusions in samples AF02-11 and AF35-10 from the Gruide granite and for Type 1 in sample AF33-10 from the Loch Shin granite.

Figure 13) Photomicrographs of Type 1 and Type 3 inclusions within quartz grains in sample AF35-10 (Gruide granite) analysed under Laser Raman Spectroscopy. Type 1 two-phase liquid-rich aqueous inclusions distributed in isolated cluster **(a)** and trails **(b)**. Type 3 three-phase aqueous-carbonic inclusions distributed in clusters (**c** and **d**).

Figure 14) Pressure-temperature space showing isochores for Type 1 and Type 3 fluid inclusions. Shaded area represents the field for Type 3 fluids defined by two isochores. Isochores for the lower and higher temperature Type 1 aqueous fluids are also shown and the parameters used for their construction are shown on the isochores. Proposed *P-T* path for cooling history of fluids in Grudie Granite is shown by the arrow. *P-T* field for aqueous carbonic fluids associated with the Mo mineralisation at the western end of the Galway Granite is shown for comparison after Gallagher *et al*., (1992).

Figure 15) a) 3-D summary of the spatial relationships between the Rogart, Loch Shin, Lairg and Grudie plutons (red) and brittle strike slip faults (grey) in the Loch Shin-Strath Fleet-Dornoch Firth area. **b)** Highly simplified conceptual model showing how the buried Laxford front shear zone below the Moine nappe gives rise to the Loch Shin Line of focussed Silurian magmas and overlapping dextral strike-slip faults.

Tables

Table I)U-Pb data for Loch Shin granite.

Table II) Re-Os data for molybdenite from the Loch Shin and Gruide granites.

Table III) Classification of fluid inclusion types and fluid inclusion micro-thermometric data from the Loch Shin and Gruide granites**.**

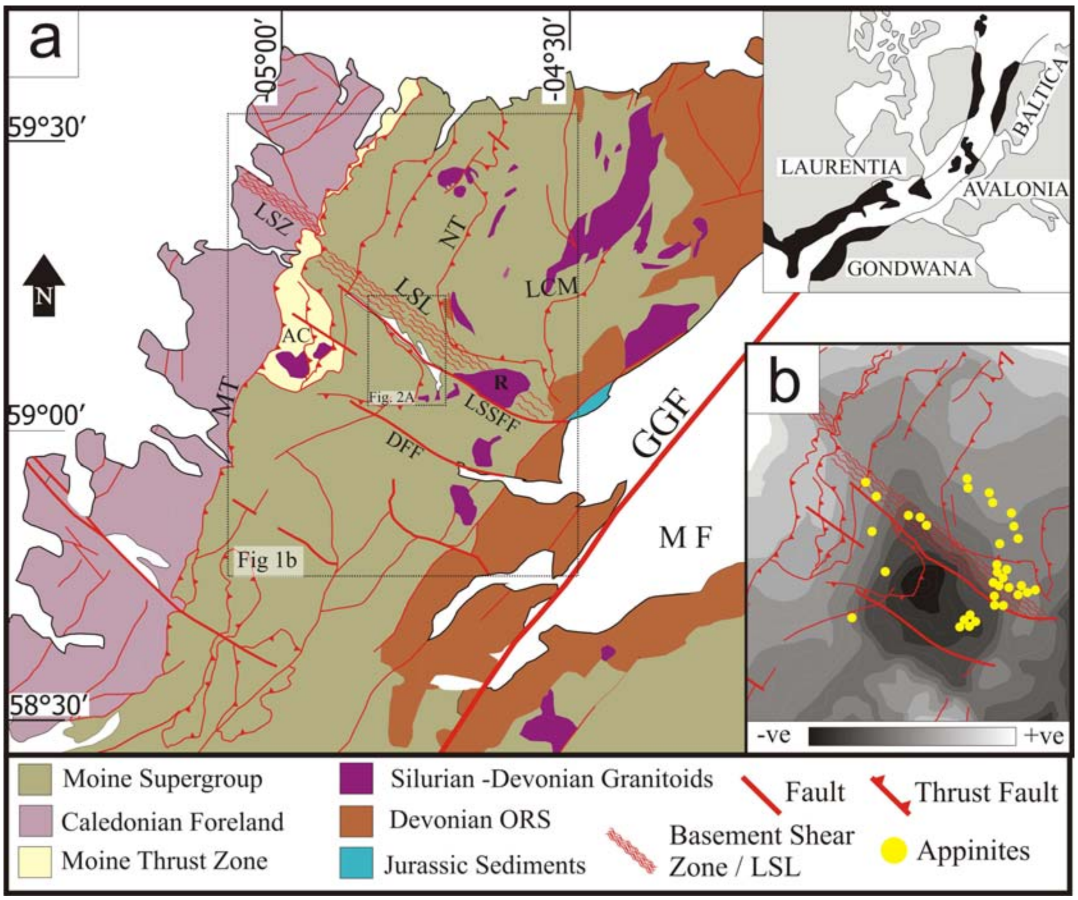

a
-05°00'
-04°30'
59°30'
59°00'
58°30'
N
LSZ
NT
LSL
LCM
AC
R
Fig. 2A
LSSFF
MT
DFF
GGF
M F
Fig 1b
LAURENTIA
BALTICA
AVALONIA
GONDWANA
b
-ve
+ve
Moine Supergroup
Caledonian Foreland
Moine Thrust Zone
Silurian -Devonian Granitoids
Devonian ORS
Jurassic Sediments
Fault
Thrust Fault
Basement Shear Zone / LSL
Appinites

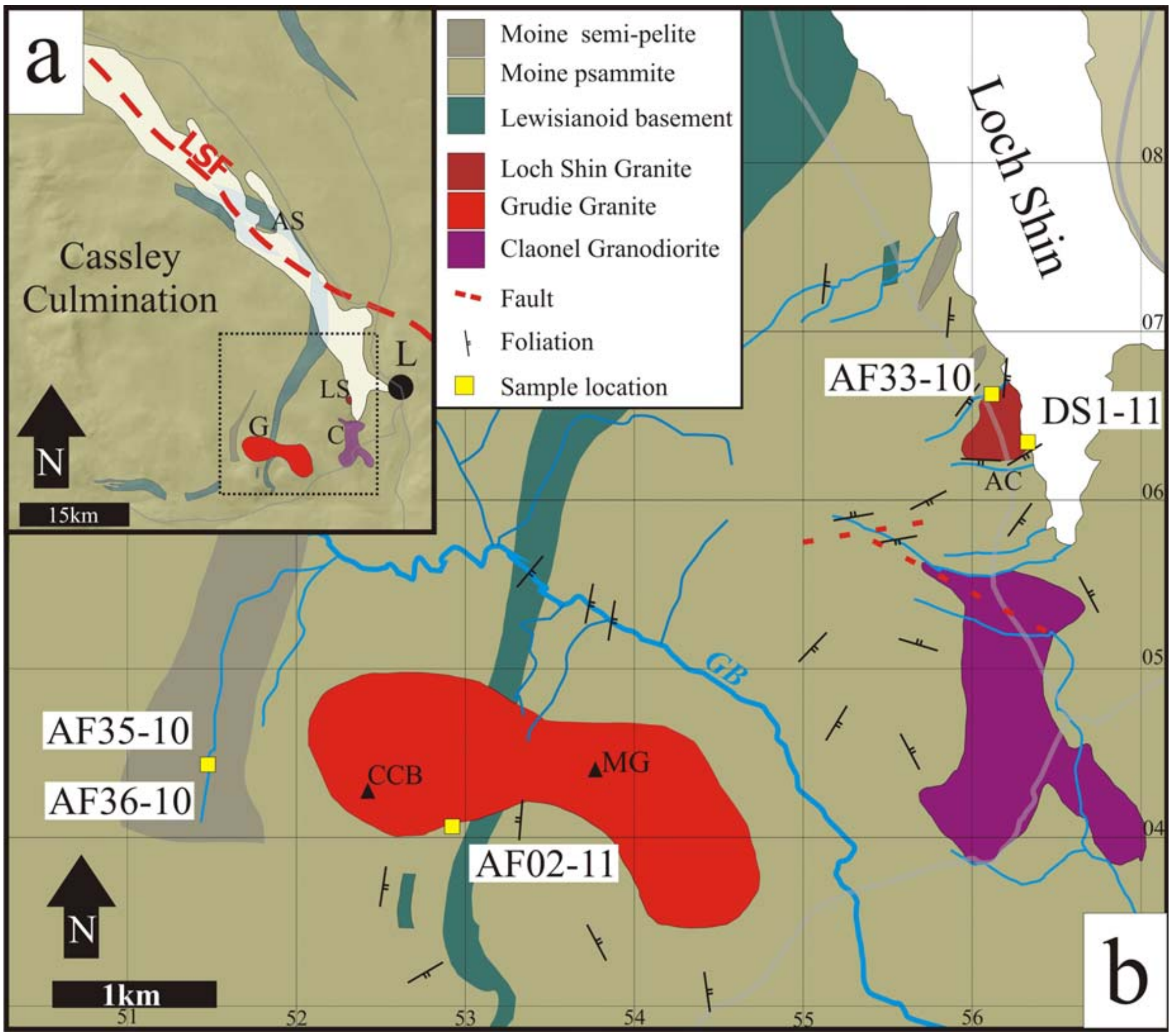
a
LSF
AS
Cassley
Culmination
L
LS
G
C
N
15km
Moine semi-pelite
Moine psammite
Lewisianoid basement
Loch Shin Granite
Grudie Granite
Claonel Granodiorite
Fault
Foliation
Sample location
Loch Shin
08
07
06
05
04
AF33-10
DS1-11
AC
GB
AF35-10
AF36-10
CCB
MG
AF02-11
N
1km
51
52
53
54
55
56
b

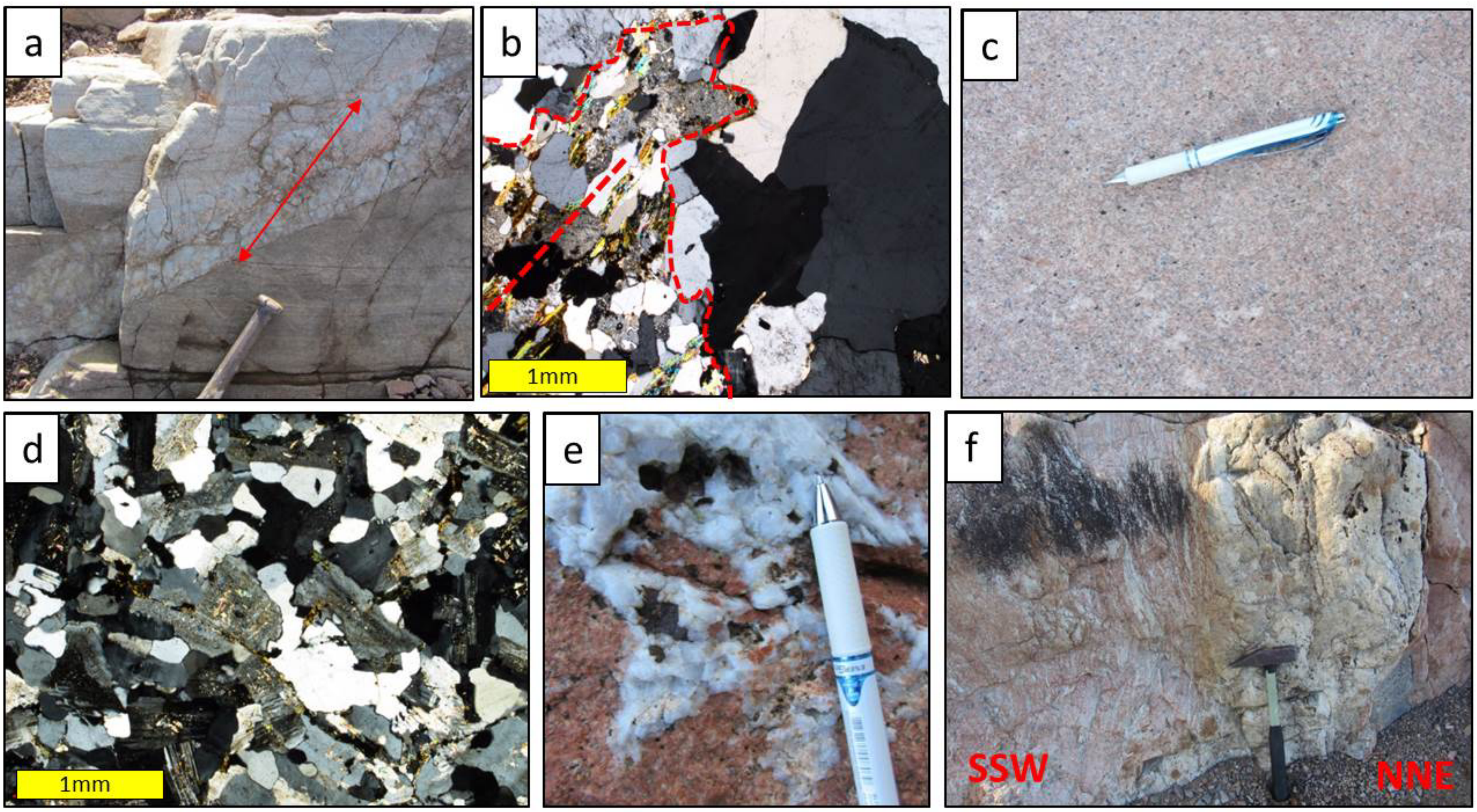
a
b
1mm
c
d
1mm
e
f
SSW
NNE

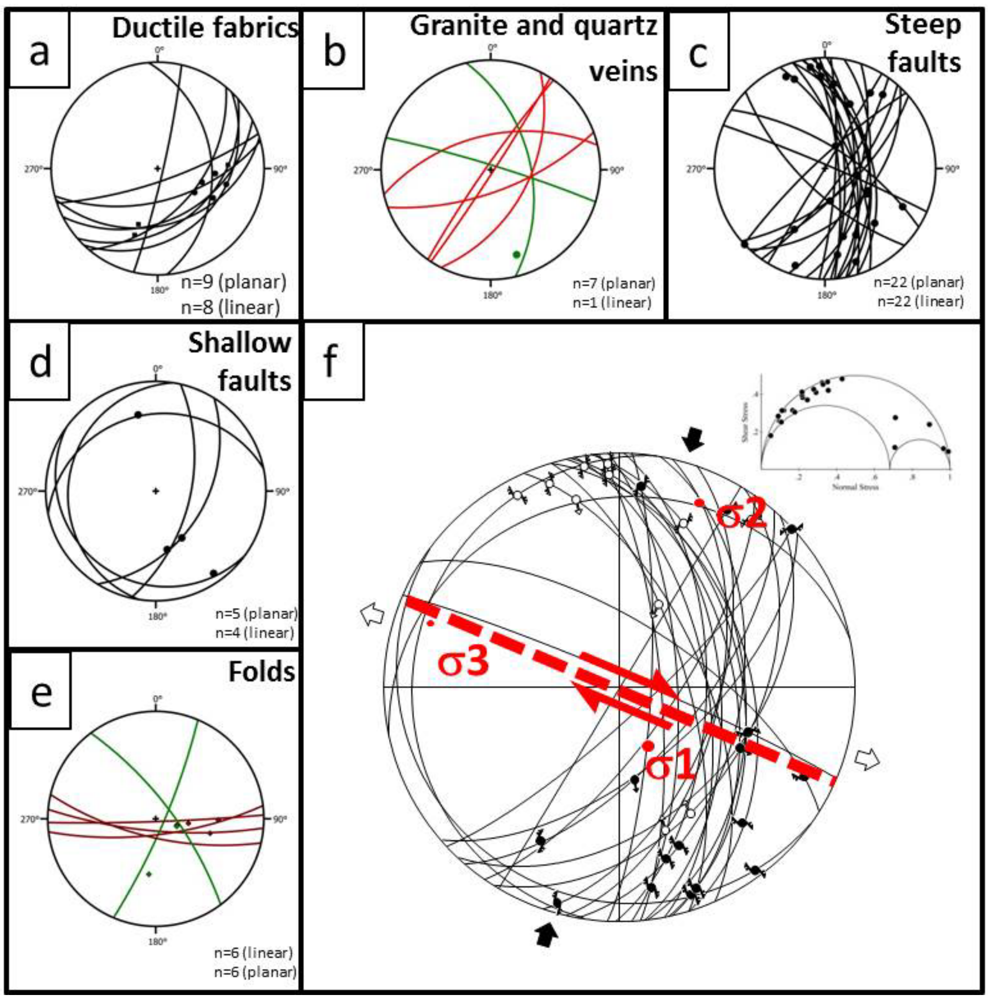

a
Ductile fabrics
0°
270°
90°
180°
n=9 (planar)
n=8 (linear)
b
Granite and quartz veins
n=7 (planar)
n=1 (linear)
c
Steep faults
n=22 (planar)
n=22 (linear)
d
Shallow faults
n=5 (planar)
n=4 (linear)
e
Folds
n=6 (linear)
n=6 (planar)
f
σ1
σ2
σ3
Shear Stress
Normal Stress

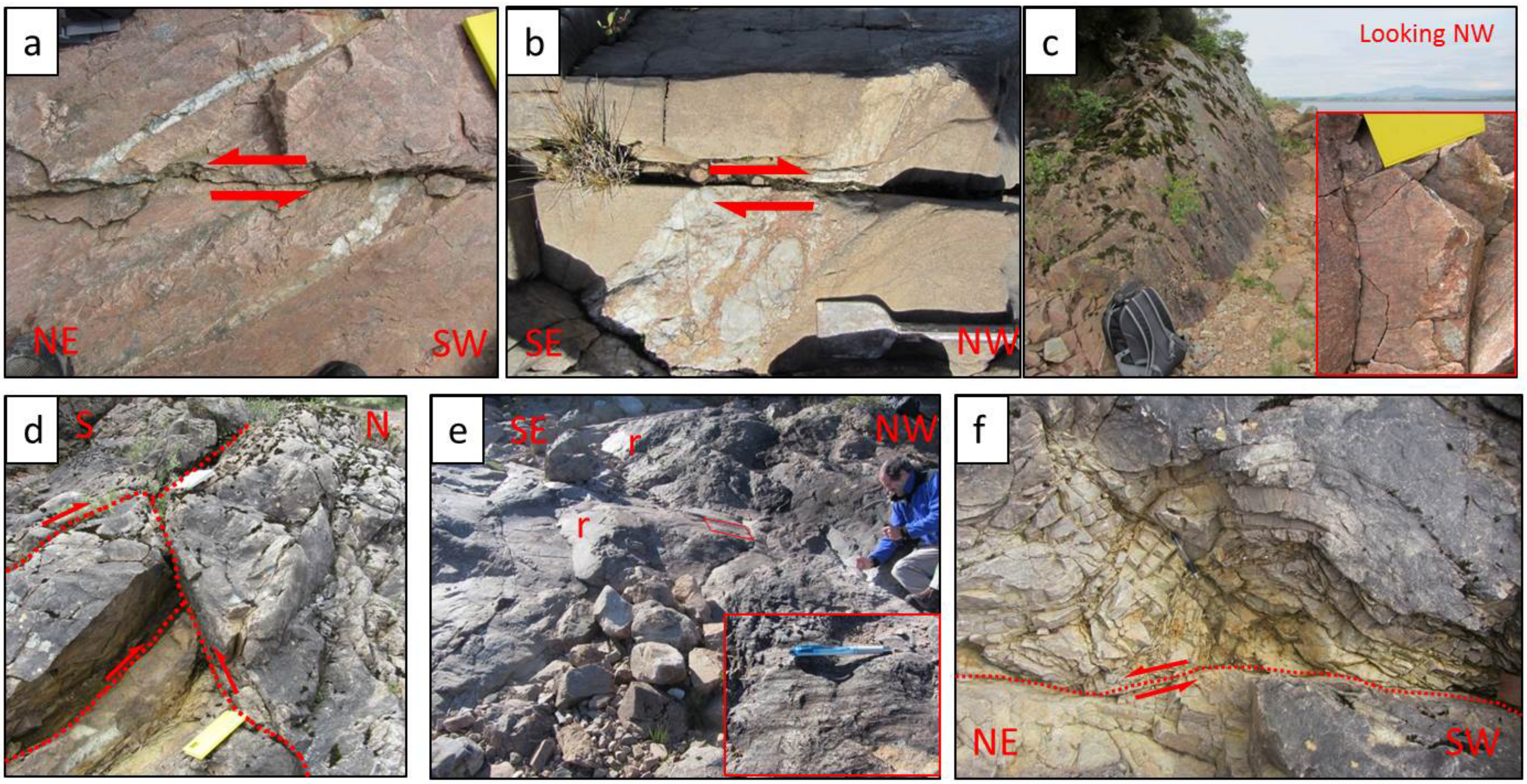
a
NE
SW
b
SE
NW
c
Looking NW
d
S
N
e
SE
NW
r
r
f
NE
SW

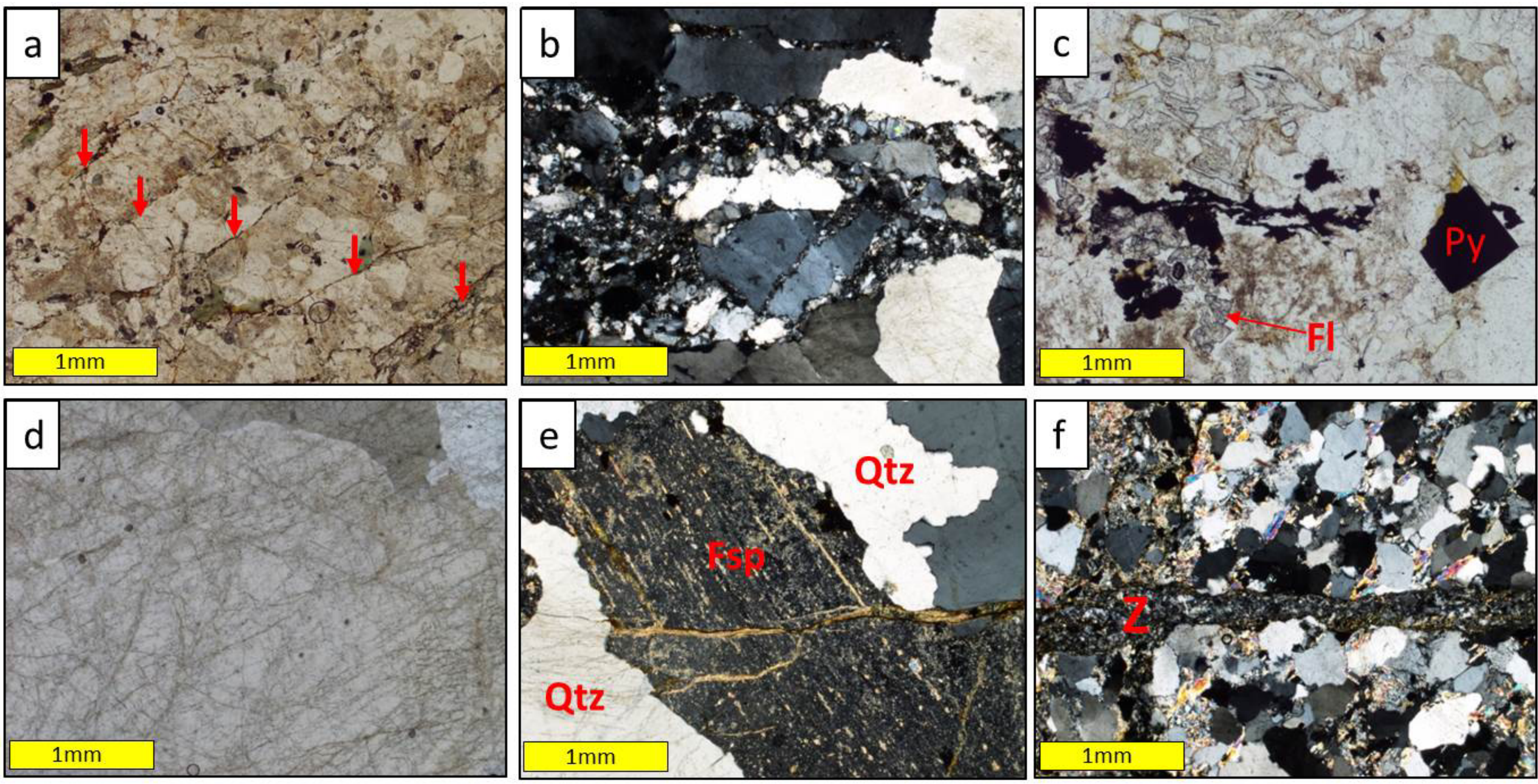
a
1mm
b
1mm
c
Py
Fl
1mm
d
1mm
e
Qtz
Fsp
Qtz
1mm
f
Z
1mm

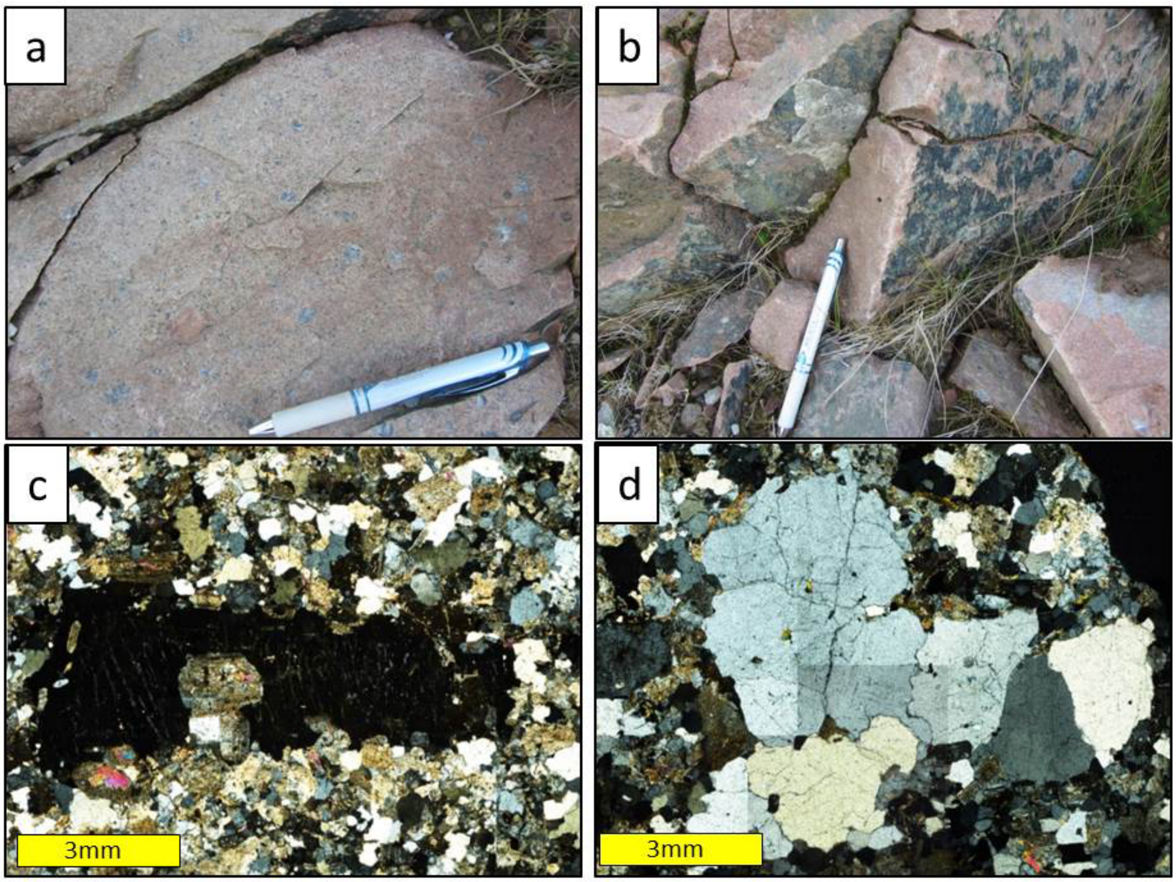
a
b
c
d
3mm
3mm

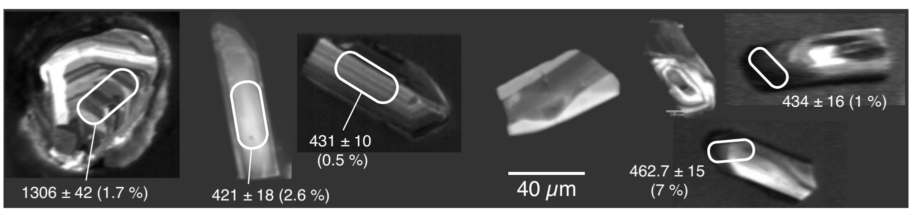
1306 ± 42 (1.7 %)
421 ± 18 (2.6 %)
431 ± 10
(0.5 %)
40 μm
462.7 ± 15
(7 %)
434 ± 16 (1 %)

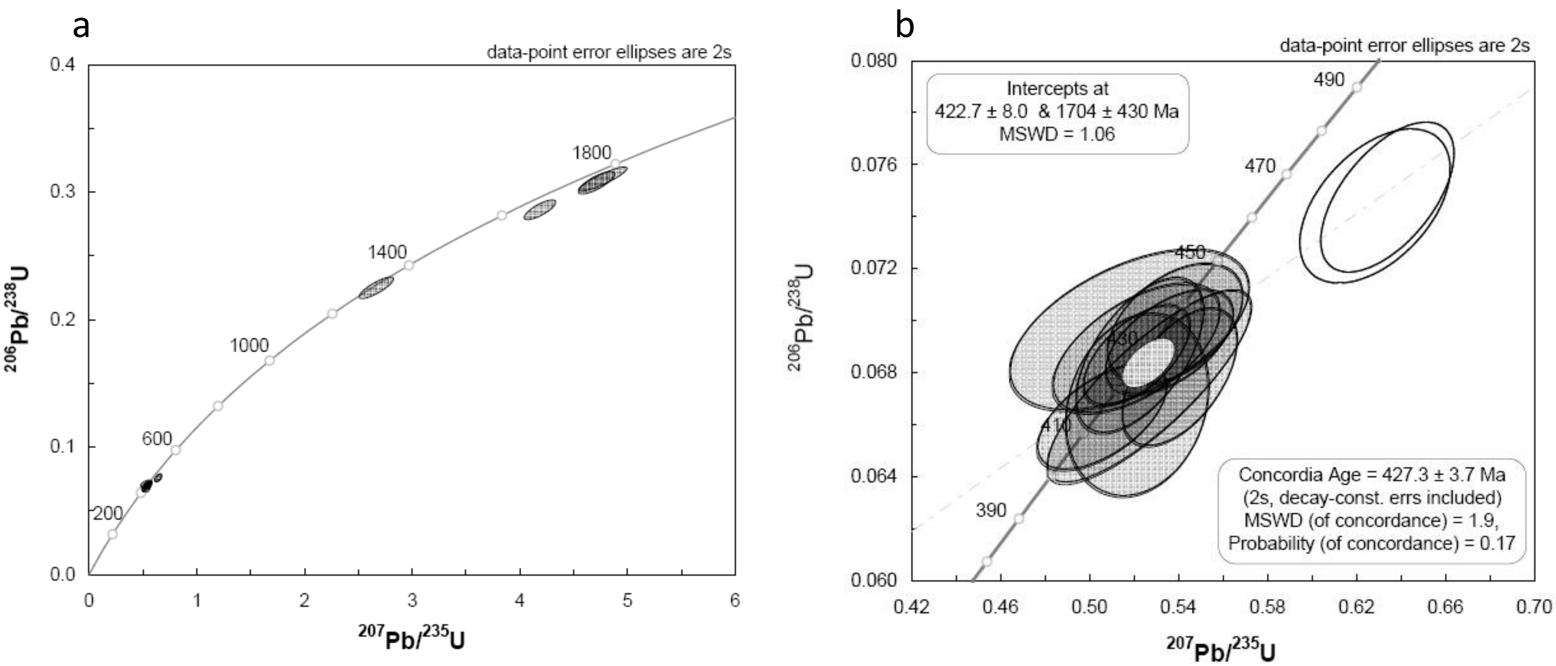
a
data-point error ellipses are 2s
0.4
0.3
0.2
0.1
0.0
$^{206}Pb/^{238}U$
1800
1400
1000
600
200
0
1
2
3
4
5
6
$^{207}Pb/^{235}U$
b
data-point error ellipses are 2s
0.080
0.076
0.072
0.068
0.064
0.060
$^{206}Pb/^{238}U$
Intercepts at
422.7 ± 8.0 & 1704 ± 430 Ma
MSWD = 1.06
490
470
450
430
410
390
Concordia Age = 427.3 ± 3.7 Ma
(2s, decay-const. errs included)
MSWD (of concordance) = 1.9,
Probability (of concordance) = 0.17
0.42
0.46
0.50
0.54
0.58
0.62
0.66
0.70
$^{207}Pb/^{235}U$

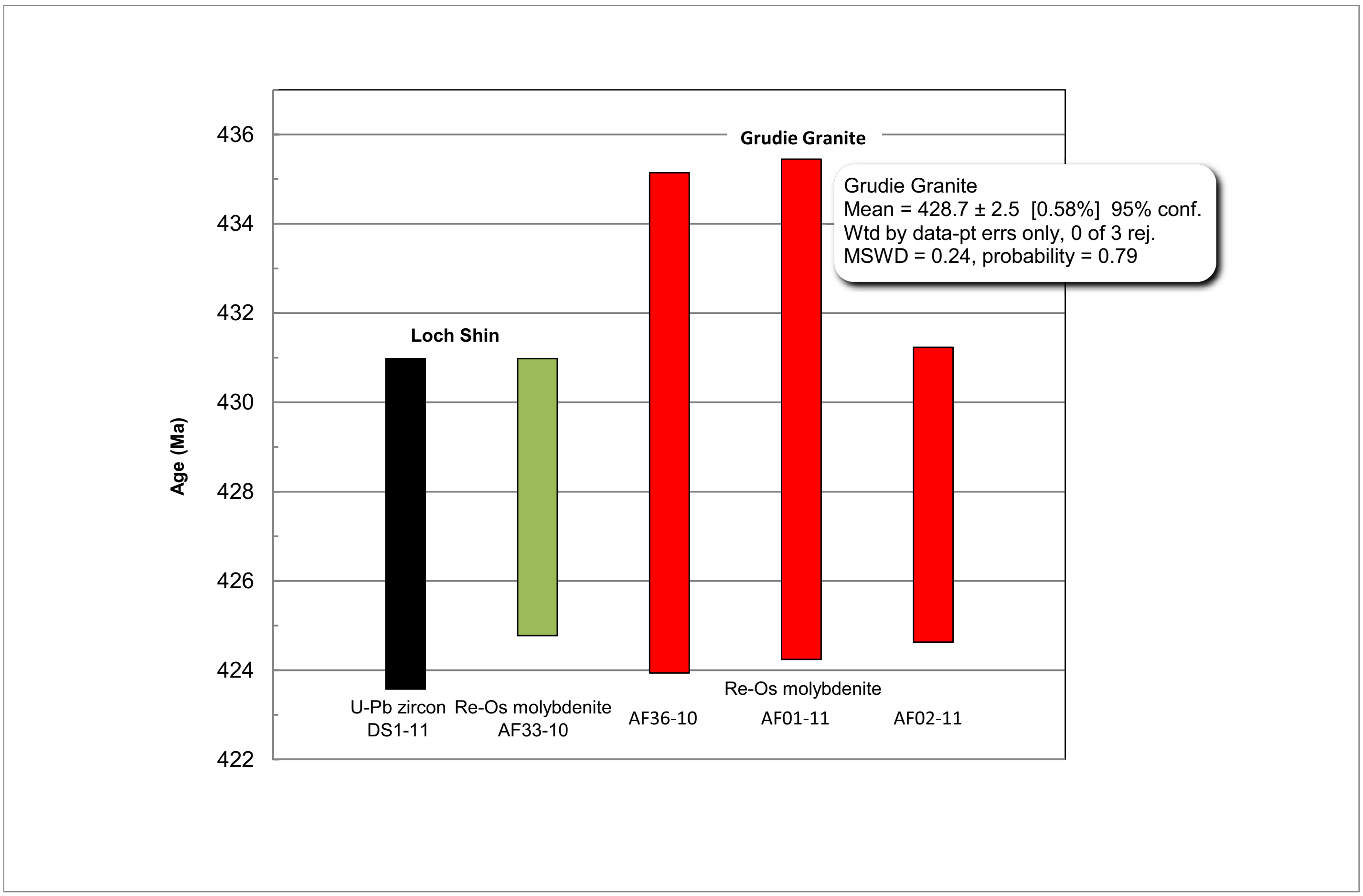
Grudie Granite
Grudie Granite
Mean = 428.7 ± 2.5 [0.58%] 95% conf.
Wtd by data-pt errs only, 0 of 3 rej.
MSWD = 0.24, probability = 0.79
Loch Shin
Age (Ma)
436
434
432
430
428
426
424
422
U-Pb zircon
DS1-11
Re-Os molybdenite
AF33-10
AF36-10
Re-Os molybdenite
AF01-11
AF02-11

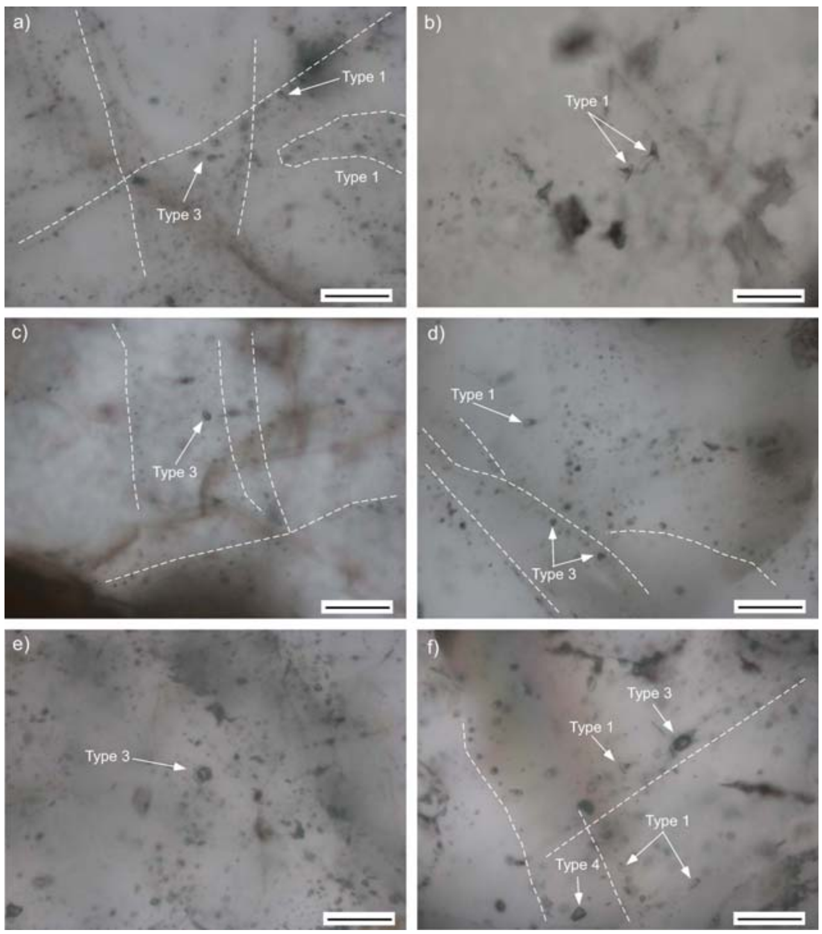

a)
Type 1
Type 1
Type 3
b)
Type 1
c)
Type 3
d)
Type 1
Type 3
e)
Type 3
f)
Type 3
Type 1
Type 1
Type 4

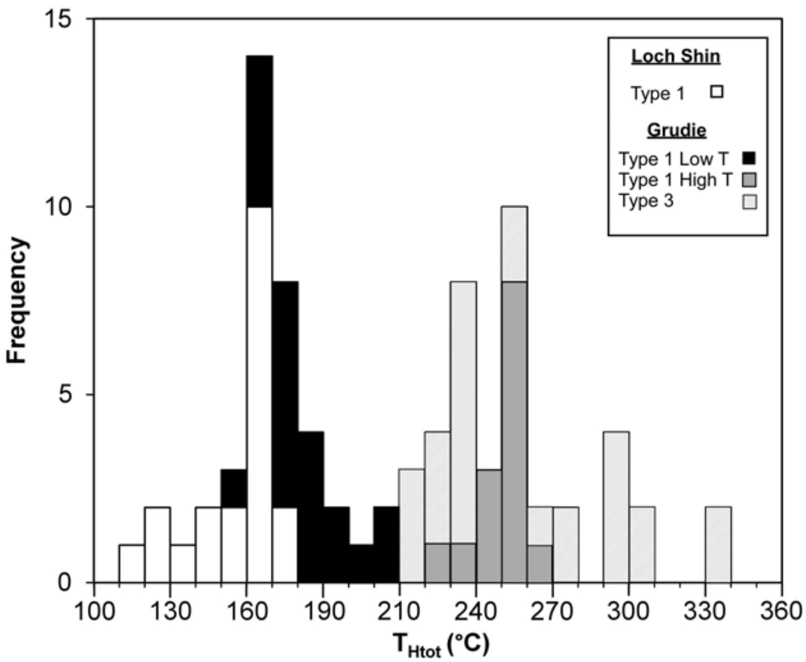

Frequency
T_Htot (°C)
Loch Shin
Type 1
Grudie
Type 1 Low T
Type 1 High T
Type 3

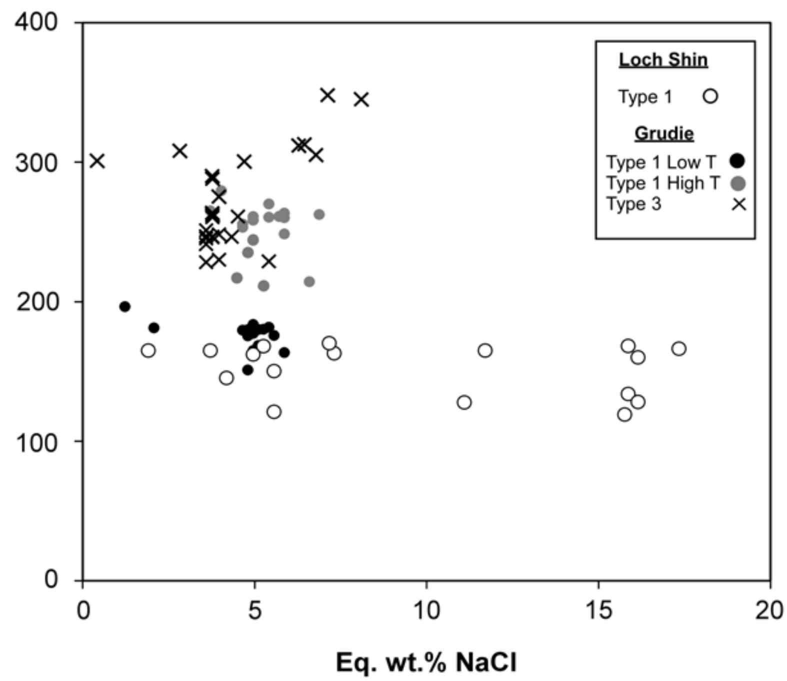

Eq. wt.% NaCl
Loch Shin
Type 1
Grudie
Type 1 Low T
Type 1 High T
Type 3

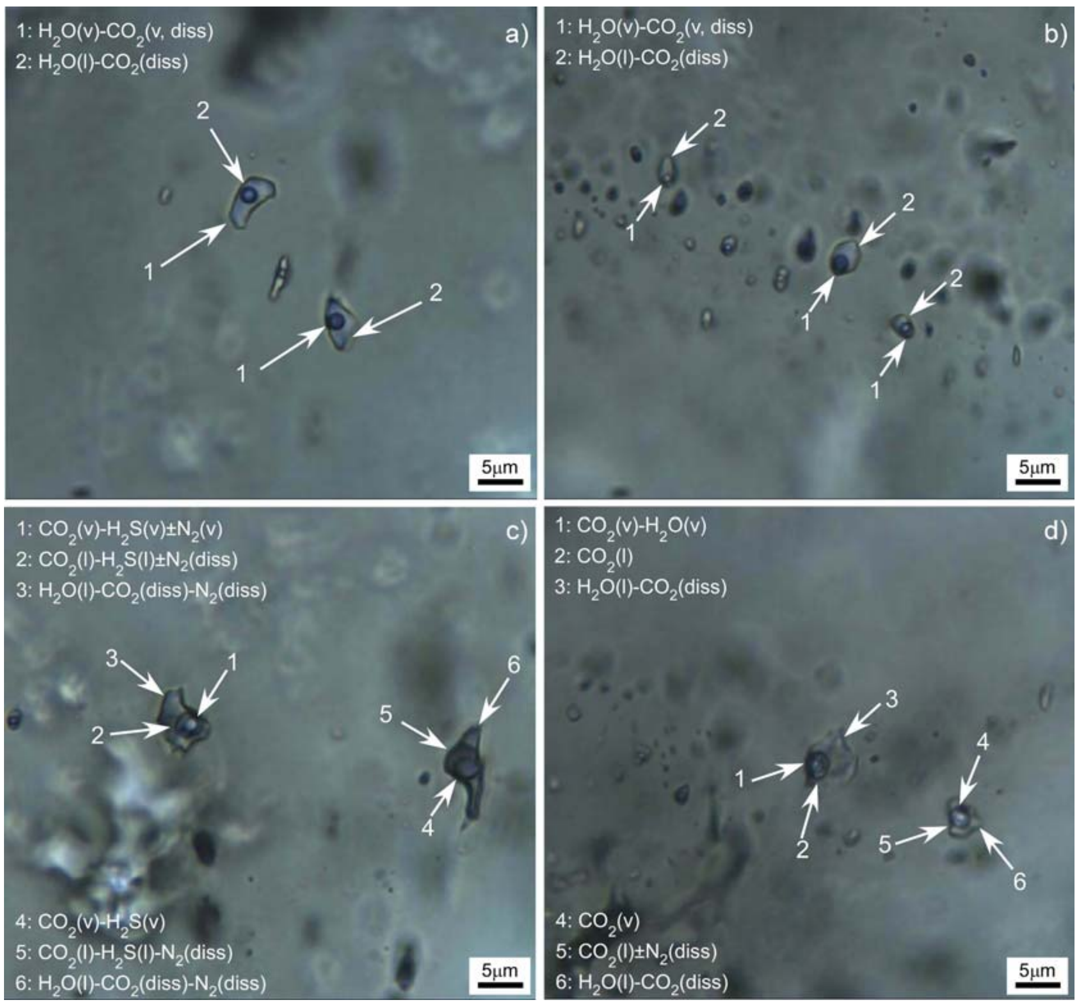

1: H2O(v)-CO2(v, diss)
2: H2O(l)-CO2(diss)
a)
5µm
1: H2O(v)-CO2(v, diss)
2: H2O(l)-CO2(diss)
b)
5µm
1: CO2(v)-H2S(v)±N2(v)
2: CO2(l)-H2S(l)±N2(diss)
3: H2O(l)-CO2(diss)-N2(diss)
c)
4: CO2(v)-H2S(v)
5: CO2(l)-H2S(l)-N2(diss)
6: H2O(l)-CO2(diss)-N2(diss)
5µm
1: CO2(v)-H2O(v)
2: CO2(l)
3: H2O(l)-CO2(diss)
d)
4: CO2(v)
5: CO2(l)±N2(diss)
6: H2O(l)-CO2(diss)
5µm

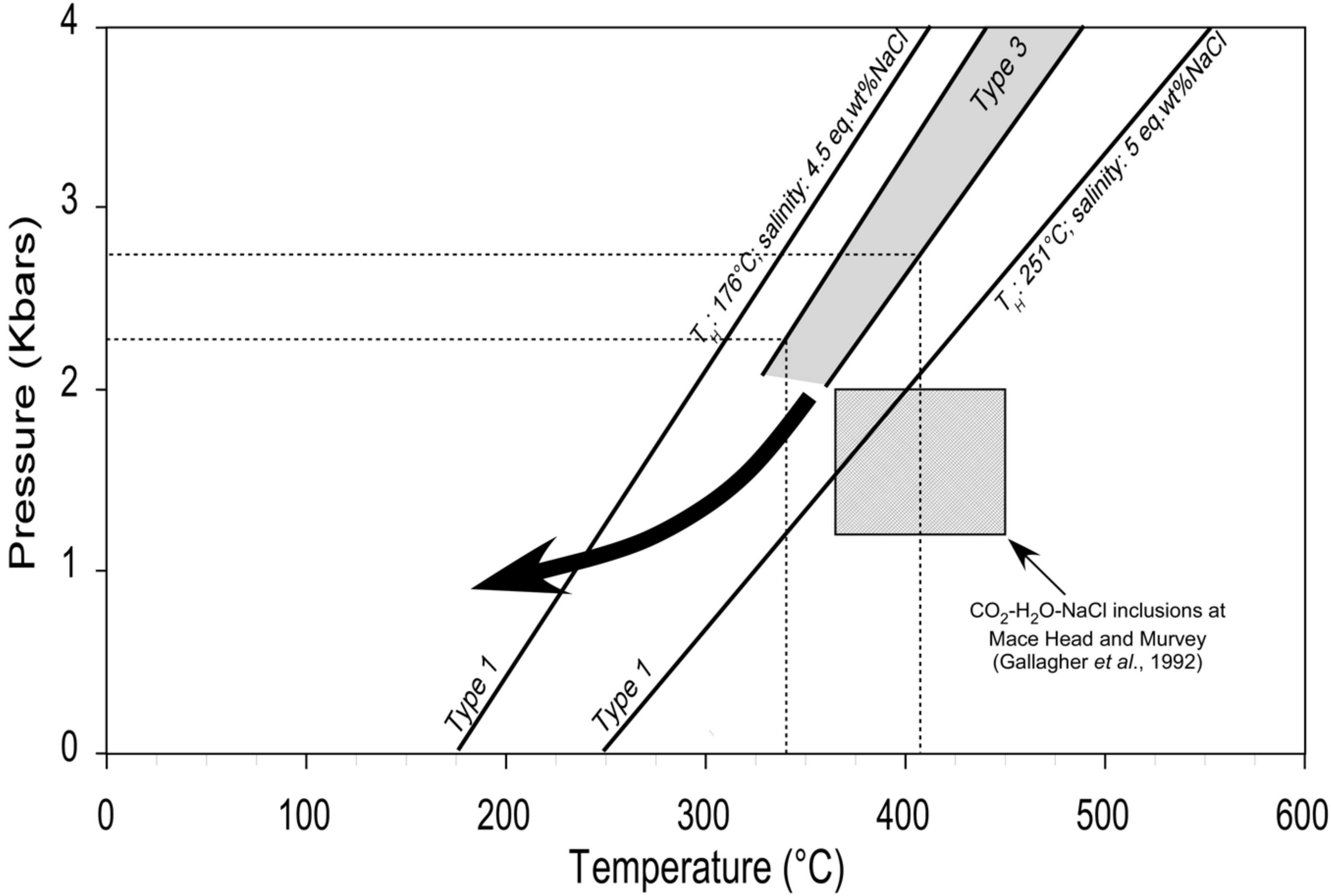

Pressure (Kbars)
Temperature (°C)
0
1
2
3
4
0
100
200
300
400
500
600
T_H: 176°C; salinity: 4.5 eq.wt%NaCl
T_H: 251°C; salinity: 5 eq.wt%NaCl
Type 3
Type 1
Type 1
CO_2-H_2O-NaCl inclusions at
Mace Head and Murvey
(Gallagher *et al.*, 1992)

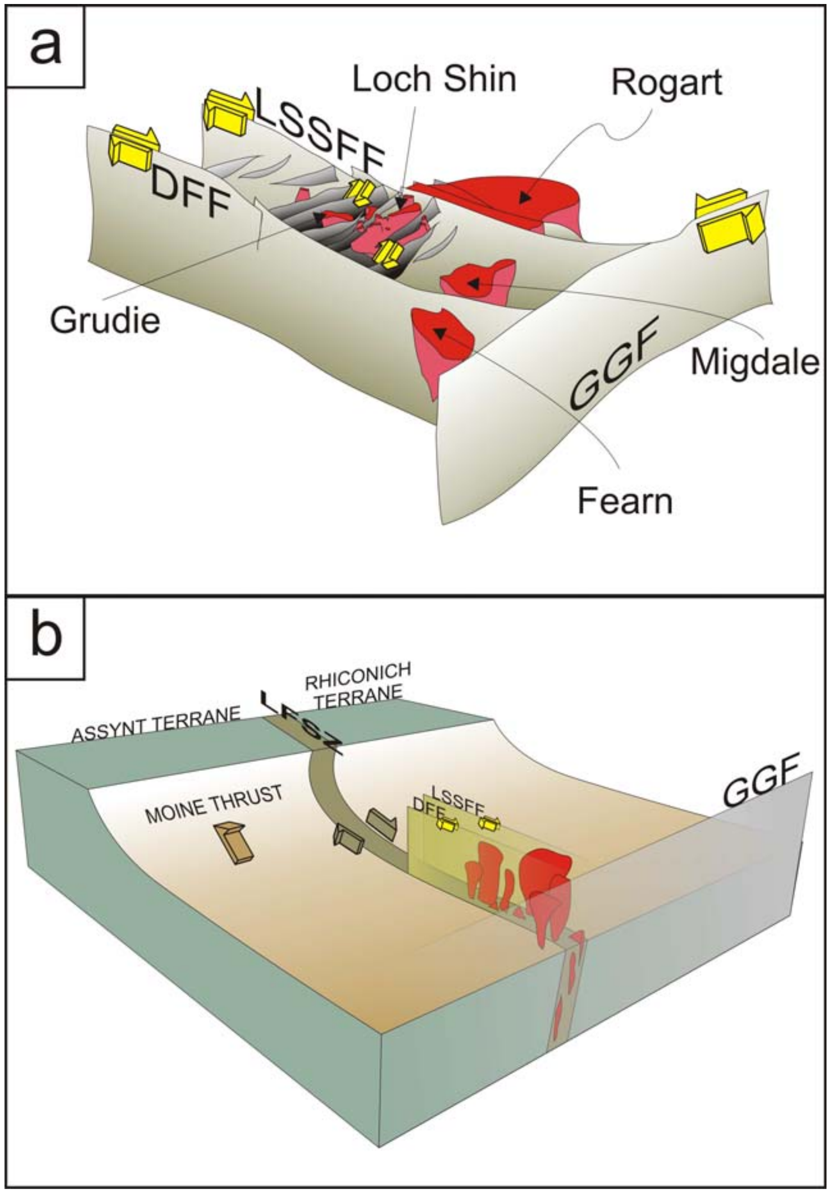

a
Loch Shin
Rogart
LSSFF
DFF
Grudie
Migdale
GGF
Fearn
b
RHICONICH
TERRANE
ASSYNT TERRANE
LFSZ
MOINE THRUST
LSSFF
DFF
GGF

School of Earth and Environmental Sciences, University of Portsmouth								Data for Tera-Wasserburg plot2				
Identifier	Comments	Beam (µm)	U (ppm)1	Th (ppm)1	Th/U	$^{206}Pb/^{204}Pb$	1s%	$^{238}U/^{206}Pb$	1σ	$^{207}Pb/^{206}Pb$	1σ	$^{207}Pb/^{235}U$
Sample DS1-11												
DE10A05		25x37	254	112	0.44	3925	37	3.494	0.039	0.106	0.001	4.188
DE10A06		25x37	208	92	0.44	2414	32	3.251	0.038	0.107	0.001	4.716
DE10A07		25x37	241	267	1.11	971	22	14.451	0.172	0.055	0.001	0.536
DE10A08		25x37	335	384	1.15	1722	37	14.558	0.258	0.056	0.001	0.523
DE10A09		25x37	105	61	0.58	2739	37	3.222	0.041	0.108	0.001	4.775
DE10A11		25x37	465	481	1.03	505	40	14.738	0.235	0.056	0.001	0.541
DE10A12		25x37	266	228	0.85	891	30	14.558	0.166	0.055	0.001	0.521
DE10A13	High 204Pb - rejected	25x37	105	161	1.54	316	32	14.490	0.197	0.071	0.002	0.695
DE10A14		25x37	51	30	0.59	790	30	4.452	0.070	0.084	0.001	2.662
DE10A15		25x37	141	154	1.1	348	27	15.079	0.188	0.056	0.001	0.506
DE10A16		25x37	282	259	0.92	1135	27	14.817	0.332	0.055	0.001	0.527
DE10B05		15x27	220	412	1.87	1814	30	14.974	0.322	0.056	0.002	0.522
DE10B06	High 204Pb - rejected	15x27	538	690	1.28	566	34	14.391	0.238	0.080	0.002	0.769
DE10B07		15x27	253	209	0.83	1225	28	13.377	0.211	0.059	0.001	0.634
DE10B08		15x27	64	77	1.19	399	30	14.353	0.260	0.055	0.002	0.518
DE10B09		15x27	123	187	1.52	615	49	14.502	0.214	0.055	0.001	0.521
DE10B10		15x27	144	191	1.33	583	33	14.305	0.193	0.056	0.001	0.539
DE10B11		15x27	290	403	1.39	1043	27	13.439	0.219	0.061	0.001	0.628
DE10B12	High 204Pb - rejected	15x27	674	1044	1.55	242	31	16.761	0.403	0.124	0.008	0.930
Standard GJ-1												
DE10AA04		30x45	389	26	0.04	1301	26	10.158	0.095	0.060	0.001	0.807
DE10AA12		30x45	266	11	0.04	1245	28	10.125	0.091	0.060	0.001	0.821
DE10AA17		30x45	310	9	0	1178	28	10.127	0.143	0.060	0.001	0.818
DE10A04		30x45	300	13	0.04	1306	27	10.133	0.086	0.060	0.001	0.828
DE10A10		30x45	292	13	0.04	1205	27	10.151	0.087	0.060	0.001	0.826
DE10A17		30x45	289	12	0.04	1441	36	10.161	0.097	0.060	0.001	0.822

DE10B04	30x45	270	12	0.04	1176	42	10.155	0.118	0.060	0.001	0.831
DE10B13	30x45	267	11	0.04	965	34	10.179	0.120	0.059	0.001	0.814
Standard Temora 2											
DE10AA05	30x45	141	83	0.6	1043	30	15.103	0.234	0.055	0.001	0.509
DE10AA06	30x45	143	85	0.6	1313	23	14.686	0.180	0.055	0.001	0.518
DE10AA07	30x45	145	86	0.6	1067	36	14.767	0.181	0.055	0.001	0.514
DE10AA08	30x45	144	100	0.7	1122	31	14.805	0.189	0.055	0.001	0.511
DE10C05	30x45	373	205	0.5	845	28	14.813	0.194	0.055	0.001	0.504
DE10C06	30x45	327	193	0.6	1187	34	14.974	0.206	0.055	0.001	0.498
De10C14	20x30	346	188	0.5	1042	34	15.231	0.177	0.055	0.001	0.504
De10C15	20x30	292	163	0.6	1063	29	15.126	0.180	0.055	0.001	0.501

1 concentration uncertainty c.20%

2 data not corrected for common-Pb

*3 Concordance calculated as (206Pb-238U age/207Pb-206Pb age)*100*

Decay constants of Jaffey et al 1971 used

Data for Wetherill plot2				Ages2						
1σ	$^{206}Pb/^{238}U$	1σ	Rho	$^{207}Pb/^{206}Pb$	1σ abs	$^{206}Pb/^{238}U$	1σ abs	$^{207}Pb/^{235}U$	1σ abs	% conc5
0.061	0.286	0.003	0.8	1725	16	1622	18	1672	25	94
0.070	0.308	0.004	0.8	1742	16	1729	20	1770	26	99
0.012	0.069	0.001	0.5	431	8	431	5	436	10	100
0.012	0.069	0.001	0.6	435	8	428	8	427	10	99
0.093	0.310	0.004	0.9	1771	18	1743	22	1780	35	98
0.011	0.068	0.001	0.5	444	8	423	7	439	9	95
0.010	0.069	0.001	0.6	427	6	428	5	426	8	100
0.023	0.069	0.001	0.8	945	22	430	6	536	18	46
0.065	0.225	0.004	0.8	1285	19	1306	21	1318	32	102
0.012	0.066	0.001	0.6	454	9	414	5	416	10	91
0.019	0.067	0.002	0.8	432	9	421	9	430	15	97
0.013	0.067	0.001	0.2	446	13	417	9	426	11	93
0.020	0.069	0.001	0.3	1209	32	433	7	579	15	36
0.012	0.075	0.001	0.6	572	9	465	7	499	10	81
0.022	0.070	0.001	0.5	429	16	434	8	424	18	101
0.015	0.069	0.001	0.6	409	10	430	6	426	13	105
0.012	0.070	0.001	0.5	436	9	436	6	438	10	100
0.014	0.074	0.001	0.5	638	13	463	8	495	11	73
0.041	0.060	0.001	-0.9	2021	134	374	9	667	30	18
0.011	0.098	0.001	0.3	594	8	605	6	601	9	102
0.014	0.099	0.001	0.4	605	9	607	5	609	11	100
0.012	0.099	0.001	0.7	609	7	607	9	607	9	100
0.011	0.099	0.001	0.6	602	6	607	5	613	8	101
0.011	0.099	0.001	0.7	613	6	606	5	611	8	99
0.012	0.098	0.001	0.7	600	7	605	6	609	9	101

0.013	0.098	0.001	0.7	590	7	605	7	614	10	103
0.013	0.098	0.001	0.7	580	7	604	7	605	10	104
0.010	0.066	0.001	0.4	429	9	413	6	418	8	96
0.010	0.068	0.001	0.4	415	8	425	5	424	8	102
0.010	0.068	0.001	0.4	426	8	422	5	421	8	99
0.010	0.068	0.001	0.4	427	8	421	5	419	8	99
0.009	0.068	0.001	0.7	417	6	421	6	415	8	101
0.009	0.067	0.001	0.7	411	6	417	6	410	7	101
0.009	0.066	0.001	0.7	416	6	410	5	414	8	98
0.009	0.066	0.001	0.6	414	6	413	5	413	7	100

Table II.

Sample	Location	wt	Re (ppm)	±	^{187}Re (ppm)	±	^{187}Os (ppb)	±	Age (Ma)	±	± (λ^{187}Re uncert)
Loch Shin											
AF33-10	Loch Shin, NC 56139, 06495	0.021	1.67	0.01	1.05	0.01	7.5	0.0	427.9	2.8	3.1
Gruide Granite											
AF36-10	Moly Burn (Gallagher & Smith, 1975), NC 51530, 04646	0.012	3.53	0.03	2.22	0.02	15.9	0.1	429.6	5.2	5.6
AF01-11	Edge of Grudie Granite NC 52726, 03797	0.014	3.40	0.03	2.14	0.02	15.4	0.1	429.9	5.2	5.6
AF02-11	Edge of Grudie Granite NC 52726, 03797	0.010	8.04	0.05	5.05	0.03	36.1	0.2	428.0	3.0	3.3

Fluid Inclusion Types	Loch Shin granite	Gruide granite	
	sample AF33-10	sample AF35-10	sample AF02-11
Type 1 two-phase (L+V) liquid-rich aqueous inclusions 9-25 µm; sub-rounded and irregular shapes; occurr in trails aligned within annealed fractures; some clusters [1]fluid composition: H_2O-NaCl±KCl±CO_2	F: 0.85-0.9 T_{FM}: -45.5° to -50.5° (mean: -47.9°C; N=7) T_{LM}: -13.5° to -1.1° (mean: -6.9°C; N=17) Salinity: 1.9 to 17.3 eq. wt%NaCl (mean: 9.7; N=17) T_H→L: 119° to 170.1° (mean: 152.9°C; N=20) Abundant	F: 0.8-0.95 T_{LM}: -3.6° to -0.7° (mean: -2.8°C; N=20) Salinity: 1.2 to 5.9 eq. wt%NaCl (mean: 4.4; N=20) T_H→L: 151° to 244.4° (mean: 185.6°C; N=20) Abundant	F: 0.7-0.9 T_{FM}: -22.5° to -23° (mean: -22.8°C; N=2) T_{LM}: -4.3° to -2.2° (mean: -3.3°C; N=20) Salinity: 3.7 to 6.9 eq. wt%NaCl (mean: 5.4; N=20) T_H→L: 214.2° to 279.5° (mean: 258.3°C; N=20) Abundant
Type 2 monophase (L) liquid aqueous inclusions 1-5 µm; rounded to sub-rounded shapes; occurr in trails within annealed fractures and randomly distributed fluid composition: H_2O-NaCl	[2]Trapping T < 50°C Abundant	Trapping T < 50°C Abundant	Trapping T < 50°C Abundant
Type 3 three- phase (L+L+V) aqueous-carbonic inclusions 4-17 µm; elongated and irregular shapes; occurr in trails aligned within annealed fractures; isolated or in clusters fluid composition: H_2O-CO_2-NaCl±H_2S±H_2	F: 0.8-0.9 Common	F: 0.8-0.9 T_{MCO2}: -57.1° to -56.5° (mean: -56.7°C; N=20) T_{Mclath}: 7.2° to 8.2° (mean: 8°C; N=18) T_{HCO2}→fading: 30.5° to 31.1° (mean: 30.8°; N=20) Salinity: 3.6 to 5.4 eq. wt%NaCl (mean: 4; N=18) Density: 0.468 g/cm^3 T_{HTOT}→L: 228.2° to 261° (mean: 243.5°C; N=20) Abundant	F: 0.4-0.85 T_{MCO2}: -57.2° to -56.2° (mean: -56.7°C; N=17) T_{Mclath}: 5.6° to 9.9° (mean: 7.2°C; N=19) T_{HCO2}→L: 28° to 30.9°; T_{HCO2}→fading 31.1° Salinity: 0.2 to 8.1 eq. wt%NaCl (mean: 4.4; N=19) Density: 0.468 to 0.655 g/cm^3 T_{HTOT}→L: 262° to 312.5° (mean: 243.5°C; N=10) T_{HTOT}→V: 305° to 348° (mean: 332.7°C; N=3) Abundant
Type 4 monophase (L) carbonic inclusions 5-10 µm; rounded to sub-rounded shapes; occurr in trails aligned within annealed fractures; some isolated fluid composition: CO_2±H_2S	Rare	Not Observed	Rare

Classification is based upon FI morphology and the volumetric proportion of phases observed at room temperature. L = liquid, V = vapour. [1]Bulk composition based on combined microthermometry and Raman spectroscopy. [2]The presence of monophase aqueous liquid FIs indicate trapping temperatures of < 50°C. ± : trace or minor constituent. T_{FM}: temperature of first ice melting; T_{LM}: temperature of last ice melting; T_{HTOT}→L: homogenisation temperature (to L); T_{HTOT} →V homogenisation temperature (to V); T_{Mclath}: temperature of clathrate melting; F: degree of fill; F=vol. liquid / (vol. liquid+vol. vapour).